Vibroacoustic Optimization of Sandwich Structures with Auxetic Cores

Mohammad Sadegh Mazloomi

Submitted to the
Institute of Graduation Studies and Research
in partial fulfillment of the requirements for the degree of

Doctor of Philosophy
in
Mechanical Engineering

Eastern Mediterranean University
December 2017
Gazimağusa, North Cyprus

Approval of the Institute of Graduate Studies and Research

Assoc. Prof. Dr. Ali Hakan Ulusoy
Acting Director

I certify that this thesis satisfies the requirements as a thesis for the degree of Doctor of Philosophy in Mechanical Engineering.

Assoc. Prof. Dr. Hasan Hacışevki
Chair, Department of Mechanical Engineering

We certify that we have read this thesis and that in our opinion it is fully adequate in scope and quality as a thesis for the degree of Doctor of Philosophy in Mechanical Engineering.

Assoc. Prof. Dr. Mostafa Ranjbar
Co-Supervisor

Asst. Prof. Dr. Neriman Özada
Supervisor

Examining Committee

1. Prof. Dr. Nizami Aktürk
2. Prof. Dr. Fuat Egelioğlu
3. Prof. Dr. Sadettin Orhan
4. Assoc. Prof. Dr. Mostafa Ranjbar
5. Assoc. Prof. Dr. Qasim Zeeshan
6. Asst. Prof. Dr. Devrim Aydın
7. Asst. Prof. Dr. Neriman Özada

ABSTRACT

This research describes the vibroacoustic behavior of sandwich structures with various core topologies. In the first part of this research a novel core topology made from 2-Dimensionally gradient auxetic hexagonal honeycombs has been proposed. The 2D gradient core enables a tailoring of localized mechanical properties of the sandwich structure in different regions of the panel. A homogenized finite element modeling is used to determine the mechanical properties of the sandwich structures. The natural frequencies and the radiated sound power level of the sandwich plate with the homogenized properties have been calculated and verified with those obtained from a exact FE model of the sandwich structure. The geometry of the 2Dimensionally gradient auxetic core has been then optimized using two different techniques in order to minimize the radiated sound power level over the frequency range of 0 to 200 Hz. The optimized design of the 2D gradient core shows a remarkable reduction of the radiated sound power level for the sandwich structure when taking into account the mass of the structures.

In the second part of this study this 2D gradient core topology concept is used in a sandwich structure with anti-tetrachiral cores. The same homogenized finite element approach is used to determine the mechanical properties of the anti-tetrachiral core and a multivariable optimization procedure is applied to minimize the radiated sound power level of the sandwich structure over the frequency range of 0 to 200 Hz. In this part a mass constrained optimization procedure is conducted. The maximum increase in the total mass is considered to be 10% of the mass of the base line configuration. The optimized structure shows a significant reduction in the radiated sound power

level accompanied by an increase in the natural frequencies of the sandwich structure.This study provides new insights about the vibroacoustic behavior of auxetic sandwich structures with complex core geometries.

Keywords: auxetic, hexagonal, chiral, anti-tetrachiral, 2D gradient, sandwich structure, vibroacoustic, optimization, genetic algorithm, MMA

ÖZ

Bu araştırmada, çeşitli temel topolojilere sahip sandviç yapıların vibroakustik davranışları incelenip analiz edilmiştir. Bu araştırmanın ilk bölümünde, 2 boyutlu (2D) auxetik altıgen peteklerden yapılmış yeni ve daha önce çalışılmamış bir temel topoloji önerisi yapılmıştır. 2D gradyan çekirdek, sandviç yapısının lokalize mekanik özelliklerini panelin farklı bölgelerinde tanımlamayı sağlamaktadır. Bu doktora tezinde, sandviç yapıların mekanik özelliklerini belirlemek için homojenize edilmiş bir sonlu elemanlar modellemesi kullanılmıştır.

Bu çalışmada, homojenleştirilmiş özelliklere sahip sandviç plakanın doğal frekansları ve ses yayılım gücü seviyesi, sandviç yapının tam ölçekli ve ayrıntılı modeli yaratılarak çalışılmış, daha sonra elde edilen sonuçlar hesaplanmış ve doğrulanmıştır. Modellemeden sonra, 2D auxetik çekirdeğin geometrisi, 0 ile 200 Hz frekans aralığı boyunca yayılan ses gücü düzeyini en aza indirgemek için iki farklı yöntem kullanılarak optimize edilmiştir.

2D çekirdeğin optimize tasarımında, panellerin kütlesi de dikkate alındığı zaman, yayılan ses gücü düzeyinde belirgin bir düşüş görülmüştür. Bu çalışmanın ikinci bölümünde, bu 2D gradyan çekirdek topolojisi, anti-tetrakiral çekirdek olarak sandviç yapıda kullanılmıştır. Bir sonraki adımda, aynı homojenize sonlu elemanlar yaklaşımı, anti-tetrakiral çekirdeğin mekanik özelliklerini belirlemek için de kullanılmıştır. Buna ek olarak, çok değişkenli optimizasyon prosedürü, 0 ile 200 Hz frekans aralığında sandviç yapının yayılan ses gücü düzeyini en aza indirmek için uygulanmıştır.

Optimizasyon sonucunda, toplam kütlenin maksimum artışı, orijinal kütlenin % 10'u olarak bulunmuştur.

Optimize edilmiş yapı, yayılan ses gücü düzeyinde sandviç yapının doğal frekanslarındaki artışa eşlik eden belirgin bir azalmayı göstermektedir. Bu çalışma, kompleks çekirdek geometrili auxetik sandviç yapıların vibroakustik davranışıyla ilgili yeni bilgiler sunmakta ve bu alanda önemli bir katkı sağlamaktadır.

Anahtar kelimeler: auxetik, altıgen, şiral, anti-tetrakiral, 2-D gradyan, sandviç panel, vibroakustik, optimizasyon, genetik algoritma

DEDICATION

This thesis work is dedicated to my loving and caring wife, Shabnam Bidmeshki, for her patience and motivation which helped me during the challenges of my Ph.D. study. I am truly thankful for having you in my life.

I also want to dedicate this work to my beloved daughter, Nikki Mazloomi.

ACKNOWLEDGMENT

I have taken great efforts in this work. However, it would not have been possible without the kind support and help of many individuals. I would like to extend my sincere thanks to all of them.

I would like to express my special gratitude and thanks to my supervisor Assist Prof. Dr. Neriman Ozada and my Co-supervisor Assoc. Prof. Dr. Mostafa Ranjbar for giving me such attention and time. This thesis would not have been completed without their expert advice and unfailing patience. I am also obliged to the jury members and especially to Assoc. Prof. Dr. Qasim Zeeshan. Without their invaluable advises all my efforts could have been short-sighted.

At the end I want to express my sincerest gratitude to Prof. Dr. Fabrizio Scarpa for giving this opportunity to conduct this research in collaboration with University of Bristol and Rolls-Royce Company.

TABLE OF CONTENTS

LIST OF TABLES

LIST OF FIGURES

LIST OF ABBREVIATIONS

ABS	Acrylonitrile Butadiene Styrene
ANN	Artificial Neural Network
ATG	Anti-tetrachiral Gradient
ERP	Equivalent Radiated Sound Power
FE	Finite Element
FEM	Finite Element Modeling
GA	Genetic Algorithm
LHS	Latin Hypercube Sampling
MMA	Method of Moving Asymptotes
NPR	Negative Poisson's Ratio
RMS	Root Mean Square
RMSL	Root Mean Square of Sound Power Level
RSPL	Radiated Sound Power Level
RUC	Representative Unit Cell
SA	Simulated Annealing
SSBC	Simply Supported Boundary Condition

LIST OF SYMBOLS

α	The ration of the horixental ligament to the oblique ligament in hexagonal honeycombs
α_x	The ratio of the ligament in x-direction to the node radius in chiral lattices
α_y	The ratio of the ligament in y-direction to the node radius in chiral lattices
b	Sandwich structure core thickness
β	The ratio of the ligament thickness to the oblique ligament length in the hexagonal honeycombs- The ratio of the ligament thickness to the node radius in the chiral lattices
C_a	Sound speed in air
E_x	Young's modulus in x-direction
E_y	Young's modulus in y-direction
E_z	Young's modulus in z-direction
E_c	Young's modulus of the core material
f	Frequency
f_{max}	Maximum frequency
f_{min}	Minimum frequency
G_{xy}	Shear modulus in xy-plane
G_{yz}	Shear modulus in yz-plane
G_{xz}	Shear modulus in xz-plane

G_{xz}^{Upper}	Upper bound for shear modulus in xz-plane
G_{xz}^{Lower}	Lower bound for shear modulus in xz-plane
G_c	Shear modulus of the core material
γ	The ratio of the core thickness to the oblique ligament length in the hexagonal honeycombs- The ratio of the core thickness to the node radius in the chiral lattice
h	The horizontal ligament length in the hexagonal honeycombs
L	The oblique ligament length in the hexagonal honeycombs
$L_s(f)$	Radiated sound power level
L_x	Ligament Length in x-direction in the chiral lattices
L_y	Ligament Length in y-direction in the chiral lattices
L_1	Fixed length in gradient topology
m_t	The total mass of the sandwich structure
n_n	Number of nodes on the sound radiating surface
$P(f)$	Radiated sound power
P_0	Standardized reference pressure
$\overline{P}$	Normalized acoustic sound power
$P_{acoustic}$	Radiated acoustic sound power
r	Node radius in the chiral larrices
ρ_a	The density of the air
S	Area of the sound radiating surface
$\sigma(f)$	Radiation efficiency
T	Kinetic energy
t	Ligament thickness in the hexagonal honeycombs

t_l	Ligament thickness in the chiral lattices
t_s	Skin thickness
θ	Internal cell angle
θ_k	Design variables vector
$v^2_{\perp rms}(f)$	Mean squared normal velocity
$v^2_{rmsi}(f)$	Mean squared velocity at point i
υ_{xy}	In-plane Poisson's ratio
υ_{yz}	Out of plane Poisson's ratio yz-plane
υ_{xz}	Out of plane Poisson's ratio xz-plane
υ_c	Poisson's ratio of the core material
ω	Circular frequency
ω_n	Natural Frequency
ω_1	First Natural frequency

Chapter 1

INTRODUCTION

1.1 Background

Since the beginning of the industrial revolution in 18th century, the environmental noise pollution has been a problem. Cars, trains, and airplanes have intensified this problem in the last 70 or 80 years. There always have been some concerns about the effect of radiating noise from industrial or transportation sources on people health. Environmental laws and regulations have been ratified to protect the people and the environment. Other than that some equipment such as noise barriers alongside railroads, highways and airports have been used to keep the harmful effect of noise pollution away from the people. New advances in car engines and tires, train wheels, airplane engines and industrial machines are beneficial in order to reduce the noise pollution. But there remain much to be done.

On the other hand, there is a demand for lightweight designs, especially in aerospace and automotive industry in order to less energy consumption or the demand for designing faster machines in order to produce more parts per unit time or to shorten travel times. Unfortunately, these tendencies are somewhat contradictory to the demand of quiet products, since light structures tend to be noisier than heavy ones, and fast machines incline to be louder than slow ones.

In most of the cases, it is advisable to try to reduce the radiated noise in the design process rather than trying to reduce the radiated noise of designed structures and machines afterward by damping treatments and encapsulation [1]. Numerical modeling can be applied to achieve a better design in order to define problematic zones at an early stage and modify the design in order to radiate less noise. That is why structural-acoustic optimizations for reducing noise and vibration have been the focus of many research studies[2].

The focus of this study is to reduce radiated noise form sandwich structures. These structures have an extensive application in automotive and aerospace industry as they possess high stiffness-to-weight ratios [3], [4]. The core can be made of polymer, titanium, aluminum and etc. The core geometry can range from conventional hexagonal honeycombs to auxetic hexagonal honeycombs and chiral lattices. Each of this different types of cores has their own geometrical properties which can be designed in a specific way to provide desired mechanical properties. Moreover, this design can be optimized in order to minimize the radiated noise and improve the acoustical behavior.

One of the mentioned types of the core in the sandwich structure was Auxetic hexagonal honeycomb core. Auxetic materials or negative Poisson's ratio (NPR) materials, get bigger in the transverse direction when they are stretched longitudinally and become smaller when they are compressed. This type of materials have unique mechanical properties and have attracted the attention of some researchers in the past few decades.

Therefore, in this study the focus will be on reducing radiated sound power form a sandwich structure with auxetic core.

1.2 Scope and Objective of the Study

As mentioned before there is a growing demand for a reliable optimization method in order to design structures with better vibroacoustic behavior. In this thesis a 2D gradient topology is introduced for sandwich structures with auxetic cores and two different types of auxetic cores have been used as a case sample. The main objectives of current thesis are as follows:

1. Develop a 2D gradient topology for auxetic sandwich structure
2. Apply the homogenization approach for the 2D gradient topology to determine the Root Mean Square of sound power Level (RMSL) in order to reduce computational time
3. Develop an optimization scheme by integrating ANSYS with MATLAB to optimize the RMSL for the 2D gradient topology
4. Optimize the RMSL for the 2D gradient topology by applying gradient base optimization method (Method of Moving Asymptotes, MMA) and direct search method (Genetic Algorithm, GA)
5. Apply all aforementioned steps for two different class of sandwich structure's core geometries. Case 1, auxetic hexagonal honeycombs and case 2, anti-tetrachiral lattices.

1.3 Organization of the Thesis

Chapter 2 presents a thorough literature review on structural acoustic of gradient auxetic sandwich structures. Chapter 3 is dedicated to the development of homogenized modeling for two different core types of sandwich structures and verifies

the accuracy of the model. Chapter 4 provides theoretical analysis on the structural acoustics of sandwich structures. Some sets of analytical formulae are given in this chapter which later they will be used in order to calculate the radiated sound power from a sandwich structure. Consequently, Chapter 5 discusses vibroacoustic optimization of the sandwich structure with gradient auxetic hexagonal honeycomb core. Chapter 6 applies same optimization algorithm for the sandwich structures with gradient anti-tetrachiral core and finally, Chapter 7 concludes.

Chapter 2

LITERATURE REVIEW

2.1 Overview

The widespread use of the sandwich structures is attributed to their outstanding out-of-plane mechanical properties, which are directly related to their shape and topology [5]. Cellular solids with honeycomb structure can be used as a sandwich core materials in different engineering applications, such as automotive lightweight structures and biomedical as they possess low relative density and high stiffness and strength to mass ratio [6]–[8]. A typical example of a sandwich structure core is the conventional hexagonal honeycomb, in which each unit cell is made of ribs with the same length and an internal cell angle of 30º [9].

The low density of the sandwich structure makes them an excellent candidate to be used in naval industry in which high stiffness and low buoyancy are required [9]. High specific strength is advantageous in the applications that high mechanical energy absorption is in need such as crashworthy materials or packaging materials for sensitive goods [9], [10].

However, the most application of the sandwich structure is when high specific bending stiffness is required. These panels were initially used in aeronautical industry [11]. Then as they become less expensive they have been used in automobile and naval industry as well as wind turbines and civil industry [9].

2.2 Auxetic Materials

In the recent years, synthetic materials possessing negative Poisson's ratio (auxetic) have been also proposed [12]–[15]. In contrast to conventional materials, these solids called "auxetic" expand in all direction when subjected to uniaxial loading [16]. Figure 1 shows a conventional hexagonal honeycomb and a typical auxetic material subjected to a uniaxial loading.

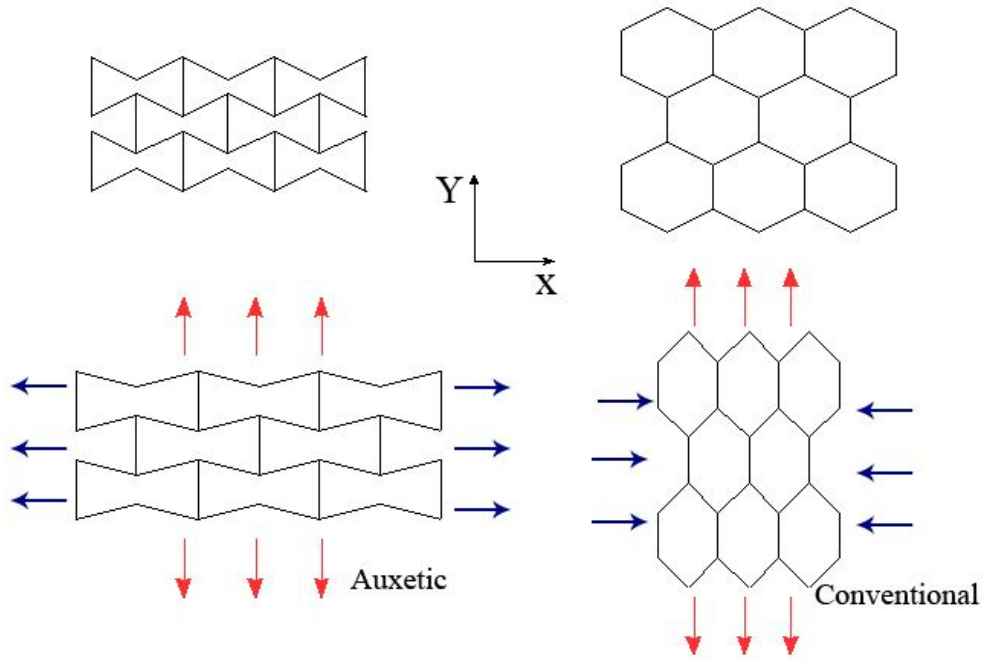

Figure 1: Conventional and auxetic honeycomb subjected to a uniaxial loading

This behavior is usually linked to specific microstructural deformation mechanisms and can be observed in several types of auxetic structures such as re-entrant, chiral, and rotating units structures [17]–[23].

2.2.1 Auxetic Hexagonal Honeycombs

One of the iconic examples of auxetic materials is the hexagonal center-symmetric re-entrant configuration [24], [25] that provides an increase in anisotropic bending stiffness, which can be useful in vibration [26] as well as for enhanced flatwise

compressive strength in reinforced butterfly cores [27]. The out-of-plane deformation of regular honeycombs shows anticlastic or saddle-shaped curvature[28]–[31]. On the other hand, structures with negative Poisson's ratio behavior exhibit synclastic curvature when subjected to out-of-plane bending which makes them an excellent candidate to be used in a complex out-of-plane geometry [8], [28], [30], [32].

2.2.2 Chiral Lattices

Another types of auxetic cellular materials are chiral lattices. Prall and Lakes [23] first, carried out a theoretical and experimental investigation of this structures. They observed that chiral lattices also show auxetic behavior as the in-plane Poisson's ratio is negative. in the case of chiral lattices, the negative Poisson's ratio gives some unique features to these structures such as a dome-shaped or synclastic bending behavior in the out-of-plane direction [29] as opposed to the conventional hexagonal honeycomb structures which show anticlastic or saddle-shaped behavior. Another distinctive feature of chiral lattices is that they show enhanced in-plane shear modulus and increased indentation resistance [33]. Figure 2 shows several types of chiral lattices.

Chiral lattices consist of circular nodes with same radii which are connected together by ligaments of equal length. The number of ligaments connected to each node is different in different types of this lattices. Three, four and six ligaments connected to each node in trichiral, tetrachiral and hexachiral lattices, respectively. In these cases, the ligaments are connected to the opposite sides of the nodes. However, in the anti-trichiral and anti-tetrachiral lattices, the ligaments are connected to the same side of the nodes.

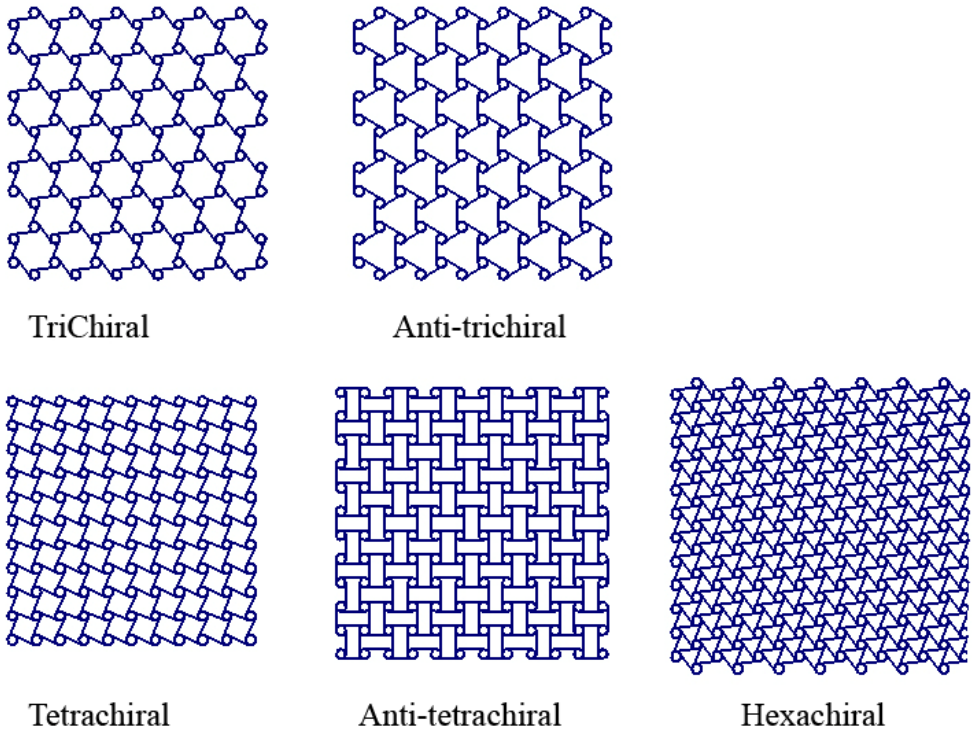

Figure 2: Different types of chiral lattices

Alderson et al [7] investigated in-plane mechanical properties of different chiral lattices using finite element modeling and some sets of experiments. They showed that Young's moduli increases with an increase in the number of ligaments connected to each node. Moreover, they reported that the tetrachiral, anti-tetrachiral and hexahiral lattices always show auxetic behavior while the anti-trichiral possessing negative Poisson's ratio for the small ratio of the ligament to the nodes radius.

Auxetic materials have been evaluated for various applications. Auxetic cellular structures have been used to prototype morphing wings [34], [35]. On the same topic, Airoldi et al. and Spadoni et al developed advanced applications of auxetic chiral structures in composite aerostructures designs [36], [37]. In another research, the wave propagation in sandwich panels with periodic auxetic core was investigated by Ruzzene et al. [38].

2.3 Homogenized Modeling

Representative unit cells have been widely used to model mechanical properties of composite materials and sandwich structures [9], [22], [39], [40]. Torquato et al [41] have applied homogenization modeling to investigate the elastic properties of regular honeycombs with triangular, square and hexagonal cells. In another study a homogenized micro-mechanical model have been used to investigate the material properties of smart composite sandwich structure with hexagonal honeycombs actuators [42]. The same concept can be applied in auxetic cellular configurations. The structure can be considered as a periodic repetition of the unit cell. The homogenized mechanical properties can also be defined by the geometrical parameters and the core properties of the repeating unit cells. Chekkal et al. [43] have used unit cell homogenization approach has to calculate the vibroacoustic behavior of auxetic structures. They showed that NPR foams perform better in acoustic absorption than the regular foams. Later Lira et al. have used homogenization approach to model an auxetic gradient cellular cores for an aero-engine fan blades [44]. Finally, Ranjbar et al. [45] have used same homogenization method to determine the mechanical properties of an auxetic hexagonal sandwich structure.

2.4 Gradient Topology

The microstructure configurations examined in the above-cited research tessellate periodically in the plane. The cellular structure is therefore made of cells having the same geometry in any part of the structure. It is, however, possible to produce this cellular structure with a gradient configuration. The configuration in this gradient topology is made of a continuous distribution of unit cells with compatible geometry, but having a single variable parameter (like the internal cell angle or internal thickness) [45]–[47]. In gradient configuration, varying distribution of stiffness and deformation

can be achieved by using a gradient cellular structure. For center-symmetric configurations, Lim introduced a varying gradient cellular topology in which the internal cell angle at each row was changing [48]. Honeycomb structures made with thickness-gradient layouts have been modeled and tested by Lira and Scarpa [49]. In particular, the cellular structures made with gradient thickness have offered an increased specific shear stiffness compared to conventional configurations with same cell shape. The flexural properties and failure behavior of sandwich structures with auxetic angle gradient core have been explored by Hou et al. [50].

Several papers have been devoted to the investigation of the vibrational and acoustic behavior of sandwich structures with normal or gradient cellular core. The vibrational characteristics of re-entrant auxetic honeycomb have been investigated by Scarpa and Tomlinson [26]. Lim [51] and Maruszewski et al. [52] have investigated the vibration of auxetic circular and rectangular plates. In another work, Shiyin et al. have studied the vibration transmission and isolation performance of trichiral structures with uniform and gradient geometry [53]. Lira et, al have used an auxetic gradient cellular as potential cores for aero-engine fan blades to reduce the dynamic response for the first three fundamental natural frequencies [44].

2.5 Structural Acoustic

One of the key parts in the design of the passive noise control compliant structure is the optimization of the structures with respect to their acoustical and structural properties (including, radiated sound power and root mean square level of the structural particle velocity). Applications and methods of structural acoustic optimization with respect to passive noise control have been reviewed by Marburg [54]. Howell et al. compared sound absorption of NPR and regular foams and reported

that NPR foams perform better in case of sound absorption [55]. Radiated sound power from a vibrating compressor was minimized conducting an acoustic topology optimization by Zhang et al. [2]. The optimization procedure was applied by modifying the local stiffness at various locations on the surface of the structure. Ruzzene [56] proposed a new configuration for a sandwich beam with honeycomb core which shows an interesting acoustic and structural characteristics. He considered the honeycomb geometry to be laid out through the thickness of the beam as shown in Figure 3. Then, he used finite element modeling to analyze the acoustic performance of the beam with various core configurations. A comparison was carried out on sound transmission reduction of the beams with various cores. The results of this study have shown that auxetic honeycombs configuration are generally more effective for reducing the sound transmission.

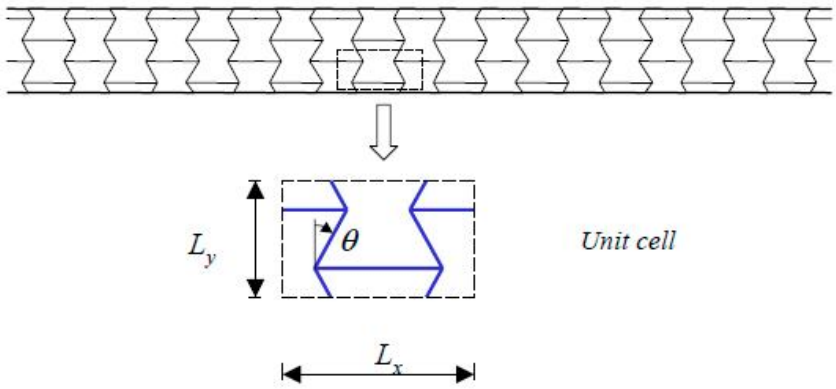

Figure 3: The proposed layout of honeycomb core [56]

Chekkal et al. [43] have investigated the vibroacoustic behavior of auxetic structures from an experimental and a numerical point of view. They showed that NPR foams perform better in acoustic absorption than the regular foams. In a totally different case, Marburg et al. [57] have used experimental and finite element approach to a certain noised transfer function for a steel box of $1\times1\times1.5$ *m* having an external beam structure

welded to it. The objective was to minimize the sound pressure at some points inside the box as a result of a force excitation on the beam. Figure 4 shows the steel box and the positions of the 3 microphones inside the box to measure the sound pressure at point M_1, M_2 and M_3.

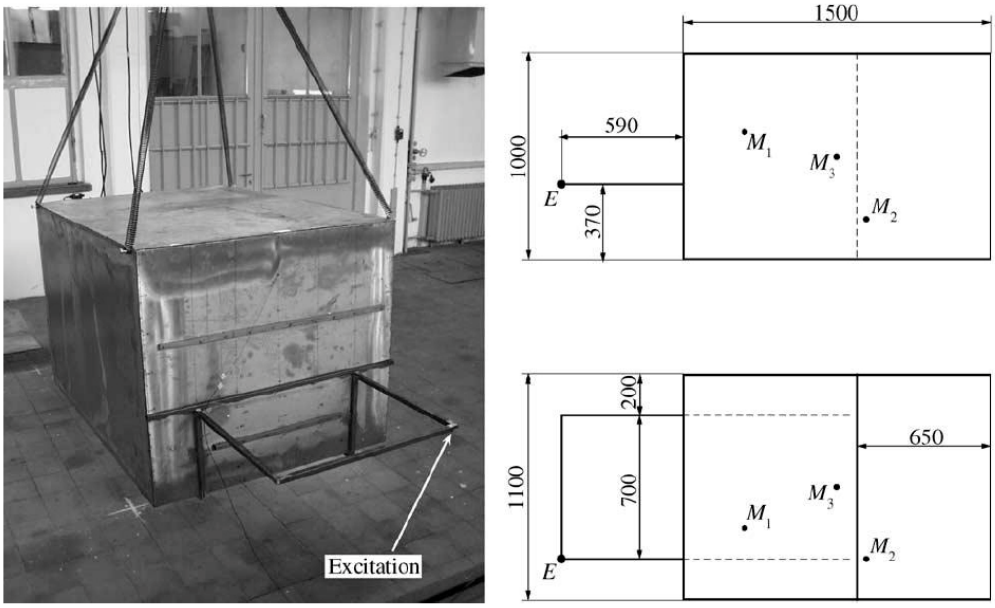

Figure 4: The steel box and the position of 3 microphones [57]

Tinstten [58] investigated the numerical acoustic optimization of a closed cylinder. Both the bottom plate and the wall of the cylinder were considered to be rigid, i.e. top plate was the only vibrating part. An excitation force with constant frequency of 600 Hz was applied on the center of the top plate. The design variables of the optimization problem were the thickness of the top plates at the different distances from the center and the objective function was sound intensity at the defined point above the top plate. Then, it was formulated as: minimized the sound intensity at the specified point when the mass of the top plate does not increase by more than 10%. The Method of Moving Asymptotes, (MMA), [59] was applied to conduct the optimization process. Figure 5

shows the point for sound intensity measurement and the initial and optimal thickness distribution.

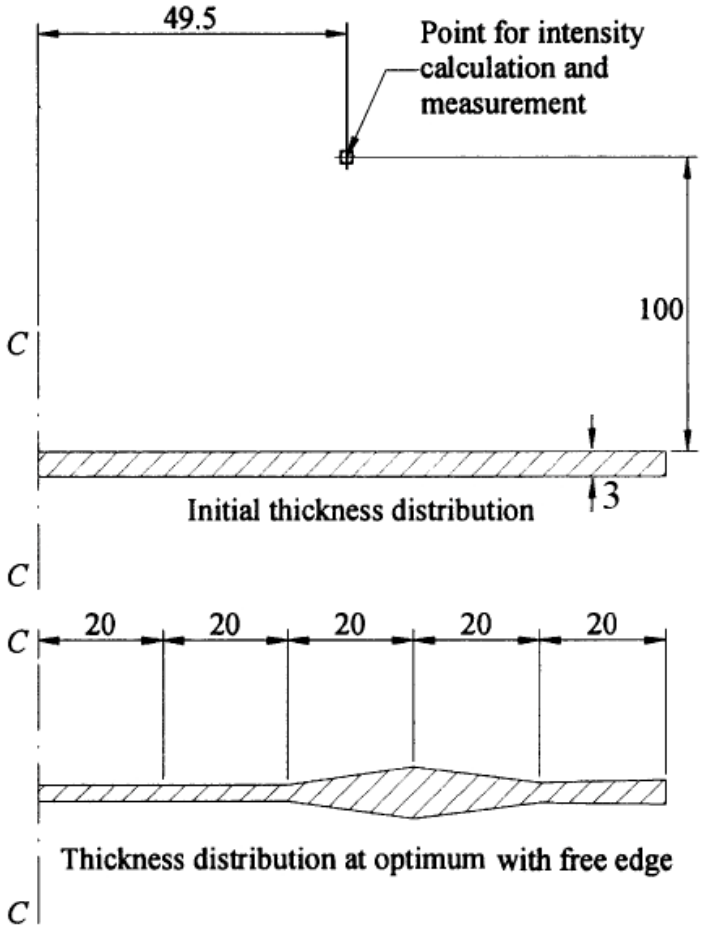

Figure 5: Initial and optimal thickness distribuation [58]

Droz et al. [3] have carried out vibroacoustic optimization of sandwich structure using a wave based finite element method. Their methodology did not require the homogenization method proposed by Gibson and Ashby [9]. They showed that auxetic periodic hexagonal honeycombs can be used to reduce the modal density in a given frequency range. Ranjbar et al. applied different optimization methods to minimize the radiated sound power level (RSPL) of a rectangular steel plate [60]–[65]. The dimension of the plate was 1×1 *m* and the thickness of the plate was considered to be *1 mm*. Instead of considering a simple flat plate they defined 9 design points as shown in Figure 6 .The height of these design points can vary between *- 1* and *+1 mm*. Having

these design points with various height leads to changing bending stiffness of the plate. They have applied a local excitation force as shown in Figure 6 and optimized the radiated sound power from the plate using a tabu search approach.

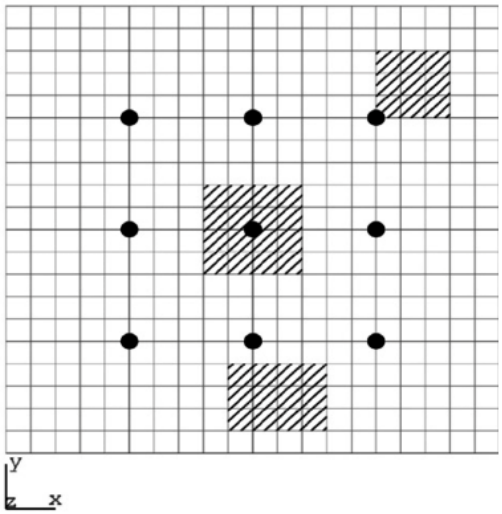

Figure 6: Rectangular palte, the design points are shown with a circle and the dashed areas are the excitation force [60]

Ranjbar et al. have also applied a combination of Artificial Neural Network (ANN) and Simulated Annealing (SA) optimization process in order to do minimize the RSPL from the mentioned rectangular plate [61]. They have also conducted the optimization process using Genetic Algorithm [62] , a controlled random search approach [63] and a hybrid simplex method optimization and design of experiments approach [64] and finally they have compared the results of all these various optimization techniques [65].

Geometrical parameters of normal and gradient auxetic cellular cores can be tailored to have desired mechanical and density properties. Therefore, they can be a suitable platform to design structural panels with optimized mechanical and vibroacoustic performance over a range of frequency bandwidths. In a different study, Ranjbar et al.

[45], studied the effect of geometrical parameters of the auxetic core on the RSPL of sandwich panel structures. Some simple optimization techniques (such as random and first order optimization method) have been used in particular to minimize the RSPL for a sandwich structure with a one-dimensional gradient auxetic core.

2.6 Concluding Remarks

Table 1 shows a tabular literature review of the most related researches in the field.

Table 1: Tabular literature review of the most related researches

No.	Research	Objective	Case sample	Optimization Method
1	Spadoni et al., 2006 [37]	predict frequency response function to investigate localized deformation	Sandwich beam, with hexachiral lattice core	No optimization
2	Howell et al., 1991 [55]	compare sound absorption of NPR and regular foams	NPR and regular foams	No optimization
3	Marburg, 2002, [54]	measure Sound intensity on a defined point	steel box of $1\times1\times1.5$ m	No optimization
4	Tinnsten, 2000, [58]	sound intensity at the defined point above the top plate	closed cylinder	MMA
5	Ruzzene et al., 2002, [38]	Investigate wave propagation in sandwich structures	NPR sandwich structure	No optimization
6	Droz, 2016, [3]	Compare modal density of various core configuration	honeycomb sandwich structure	No optimization
7	Chekkal et al., 2010, [43]	Compare acoustic absorption of the NPR foams and the regular foams	NPR and regular foams	No optimization
8	Ruzzene, 2004,	Comparing sound transmission reduction of the sandwich beams with various cores	Sandwich beam with various core topologies	No optimization

No.	Research	Objective	Case sample	Optimization Method
9	Lira et al., 2011, [44]	Minimize modal mass displacement	gradient aero-engine fan blade	first order
10	Lira & Scarpa, 2010, [49]	Determining transverse shear stiffness of thickness gradient honeycombs	Thickness gradient hexagonal honeycombs	No optimization
11	Hou et al., 2013, [50]	bending and failure behavior of gradient honeycomb	Ligament gradient hexagonal honeycombs	No optimization
12	Shiyin et al., 2015, [53]	Investigate isolation performance of the trichiral structures	Uniform and gradient trichiral structures	No optimization
13	Zhang et al., 2017, [2]	minimizing RSPL	compressor housing	Not mentioned
14	Marburg & Ranjbar, 2012, [62]	minimizing RSPL	rectangular steel plate	Genetic Algorithm
15	Ranjbar, 2013, [61]	minimizing RSPL	rectangular steel plate	ANN&SA
16	Ranjbar & Marburg, 2012, [63]	minimizing RSPL	rectangular steel plate	Random search
17	Ranjbar et al., 2011, [64]	minimizing RSPL	rectangular steel plate	Hybrid simplex &DOE
18	Ranjbar et al., 2016, [45]	minimizing RSPL	1-D gradient hexagonal honeycomb sandwich structure	Random& first order

The extensive review of the literature shows that although there have been some sets of researches on the effect of topology optimization on the acoustical behavior of the

rectangular plates and effect of core topology of the sandwich structures on their vibrational behavior, there are still a number of gaps in acoustical behavior of sandwich structures with auxetic gradient cores. In the present research, we investigate the effect of the topology of a novel two-dimensional gradient auxetic honeycomb core on the RSPL. Moreover, two well-known and robust optimization methods, i.e. the genetic algorithm (GA) and the Method of Moving Asymptotes (MMA) [59], [66] are applied to minimize the RSPL from the sandwich structure. To perform this analysis a direct software coupling between MATLAB and ANSYS [67] (Finite Elements) software platforms has been developed. To the best of the Author's knowledge, a 2D gradient cellular auxetic topology has not been thoroughly evaluated for vibroacoustic applications. Moreover, the use of a combined GA-MMA optimization approach is a first in the field of vibroacoustic.

Chapter 3

STRUCTURAL MODELING

3.1 Introduction

This chapter describes the methodology used to model the sandwich structure core as an orthotropic material. An appropriate method which can be used to model the core material is homogenization method. In order to simulate the sandwich structure, one can model the detailed geometry of the core considering all the geometrical parameters. However, there will be a large number of elements in the exact FE modeling causing a big increase in the total computational time. As one of the objectives of this research is to implement optimization algorithms to minimize the RSPL and the optimization algorithms are iterative procedures, this large computational time will serve as a key obstacle. Therefore, the total computational time should be decreased. The homogenized FE modeling can be used to model the sandwich structure core as an orthotropic material with defined mechanical properties. In the section 3.2, the application of this homogenized modeling for the case 1 of this study which is auxetic hexagonal honeycomb have been proposed. Section 3.3 propose the same methodology for the case 2 of this study which is anti-tetrachiral lattices.

3.2 Homogenization Modeling of the Auxetic Hexagonal Honeycomb

Homogenized modeling have been used previously for the sandwich structures. Gibson and Ashby [9] have proposed some closed form formulae to predict the mechanical properties of center-symetric hexagonal honeycombs. These formulae later have been used by Lira et al. [44] to determine mechanical properties of an aero-

engine fan blade with an auxetic hexagonal honeycomb core. In the following section, the mechanical properties of hexagonal honeycombs have been calculated.

3.2.1 Mechanical Properties of the Hexagonal Honeycomb

In these sets of formulae, the mechanical properties of the core have been defined with their geometrical parameter. Figure 7 shows a unit cell for the auxetic hexagonal honeycomb with its geometrical parameters.

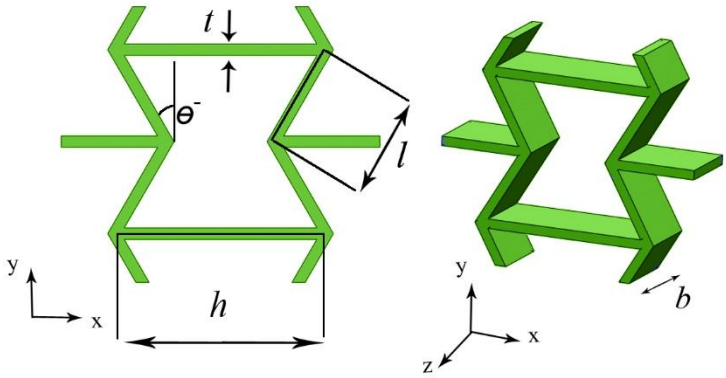

Figure 7: A Representative Unit Cell (RUC) of the auxetic hexagonal honeycomb

Later, Lira et al. [44] and Ranjbar et al. [45] have used the same analytical method which defines mechanical properties of hexagonal honeycombs based on three non-dimensional parameters $\alpha = \frac{h}{l}$, $\beta = \frac{t}{l}$, $\gamma = \frac{b}{l}$ and the angle θ. The In-plane and out of plane mechanical properties of the hexagonal honeycomb are defined as follows.

$$E_x = E_c \beta^3 \left(\frac{\alpha + \sin\theta}{\cos^3\theta \left[1 + (2.4 + 1.5\upsilon_c + \tan^2\theta + \frac{2\alpha}{\cos^2\theta})(\beta^2) \right]} \right) \tag{1}$$

$$E_y = E_c \beta^3 \left(\frac{\cos\theta}{\sin^2\theta(\alpha + \sin\theta)[1 + (2.4 + 1.5\upsilon_c + \cot^2\theta)(\beta^2)]} \right) \tag{2}$$

$$\upsilon_{xy} = \left(\frac{\cos^2\theta}{\sin\theta(\alpha + \sin\theta)} \right) \left(\frac{1 + (1.4 + 1.5\upsilon_c)(\beta^2)}{1 + (2.4 + 1.5\upsilon_c + \cot^2\theta)(\beta^2)} \right) \tag{3}$$

$$G_{xy} = E_c \beta^3 \left(\frac{(\alpha + \sin\theta)}{\alpha^2 \cos\theta} \right) \frac{1}{F} \tag{4}$$

Where

$$F = 1 + 2\alpha + \beta^2 \left[\left(\frac{2.4 + 1.5\upsilon_c}{\alpha} \right) (2 + \alpha + \sin\theta) + \left(\frac{\alpha + \sin^2\theta}{\alpha^2} \right) \left[(\alpha + \sin\theta)\tan^2\theta + \sin\theta \right] \right] \tag{5}$$

$$E_z = E_c \beta \left(\frac{\alpha + 2}{2(\alpha + \sin\theta)\cos\theta} \right) \tag{6}$$

$$G_{yz} = G_c \beta \left(\frac{\cos\theta}{(\alpha + \sin\theta)} \right) \tag{7}$$

For the all above mentioned mechanical properties there is a unique value. However, the value of G_{xz} is bounded between the upper (Voigt) and the lower (Reuss) bound. The upper bound and lower bound are defined as follows:

$$G_{xz}^{upper} = G_c \beta \left(\frac{\alpha + 2\sin^2\theta}{2(\alpha + \sin\theta)\cos\theta} \right) \tag{8}$$

$$G_{xz}^{lower} = G_c \beta \left(\frac{\alpha + \sin\theta}{(1 + 2\alpha)\cos\theta} \right) \tag{9}$$

Grediac [68] and later Scarpa and Tomlin [25] showed that the shear modulus G_{xz} depends the width, b, of honeycomb and for the $1 \le \gamma \le 10$ G_{xz} can be defined as follows:

$$G_{xz} = G_{xz}^{lower} + \frac{K}{\gamma}(G_{xz}^{upper} - G_{xz}^{lower}) \tag{10}$$

In which

$$K = \begin{cases} 0.787 & \theta \ge 0 \\ 1.342 & \theta < 0 \end{cases} \tag{11}$$

The mechanical properties of the honeycomb core plate are modeled by an equivalent orthotropic material. The compliance matrix [S] for an orthotropic material is defined

as below, in which the engineering constants E_x, E_y, E_z, G_{xy}, G_{yz} and G_{xz} can be found from the above formulae. Considering Cellular Material Theory [9], the out-of-plane Poisson's ratios υ_{xz} and υ_{yz} can be assumed approximately zero. Moreover, the other transverse Poisson's ratios $\upsilon_{zx}, \upsilon_{zy}$ are assumed to be equal to Poisson's ratio of the core material, υ_c [9], [44].

$$[S] = \begin{bmatrix} \frac{1}{E_x} & -\frac{\upsilon_{xy}}{E_y} & -\frac{\upsilon_{xz}}{E_z} & 0 & 0 & 0 \\ -\frac{\upsilon_{yx}}{E_x} & \frac{1}{E_y} & -\frac{\upsilon_{yz}}{E_z} & 0 & 0 & 0 \\ -\frac{\upsilon_{zx}}{E_x} & -\frac{\upsilon_{zy}}{E_y} & \frac{1}{E_z} & 0 & 0 & 0 \\ 0 & 0 & 0 & \frac{1}{G_{xz}} & 0 & 0 \\ 0 & 0 & 0 & 0 & \frac{1}{G_{yz}} & 0 \\ 0 & 0 & 0 & 0 & 0 & \frac{1}{G_{xy}} \end{bmatrix} \quad (12)$$

The formulations given in [9] for calculation of the mechanical properties of hexagonal honeycombs are valid for honeycomb panels made of at least 12×12 unit cells [44]. However, for the structures made of periodic assemblies of fewer cells, the stiffness can be generally decreased compared to the theoretical infinite panel solution [48]. In this study, each region consists 10×6 unit cells. Honeycomb panels made of at least 10×10 unit cell show substantially the same behavior of the theoretical solution under uniaxial tensile loading, while reducing the number of the unit cell to 10×6 will cause a slight reduction of stiffness E_x compared to the one predicted by the theoretic formula. However, Ranjbar et al. [45] showed that for a gradient topology, if the total number of unit cells in the whole structure is greater than 10×8, the theoretical value predicted for E_x can be considered as an adequate approximation. In this study the gradient sandwich structure is made of 18×30 unit cells; one can, therefore, infer that

the formula given by Gibson and Ashby [9] can still be used to calculate the mechanical properties of the sandwich structure core in each region.

Figure 8 shows the variation of E_x/E_c and E_y/E_c with respect to the change in the internal angle θ. In this case, E_c is the Young's modulus of the core material (ABS Plastic [49]). The figure shows that an increase in the negative angle θ causes a slight increase in E_x; conversely, an increase in E_y is more significant than one present in E_x. It is worth mentioning that an increase in the angle θ leads to a decrease of the out-of-plane Young's modulus E_z [9].

The transverse bending of the sandwich plates is mostly ruled by the out-of-plane transverse shear moduli G_{xz} and G_{yz} [10]. For center-symmetric hexagonal honeycombs, G_{yz} modulus has a unique value [9], while the G_{xz} is limited between an upper (Voigt) and a lower (Reuss) bound. The value of G_{xz} can be identified from the effect created by the through the thickness bending on the honeycomb walls [25]. Figure 9 illustrates the variation of G_{xz} and G_{yz} with the change of the cell angle. For negative angles, an increase in the magnitude of the cell angle causes a reduction on G_{xz}, while it has the opposite effect for G_{yz}. Moreover, it is worth noticing that G_{xz} is generally higher in negative angles than positive. As it can be seen in Figure 9, the in-plane Young's moduli of an auxetic hexagonal core have higher values when the cell angle is between -30 to -10 and the change in these moduli are more significant than the change in the range -50 to -30. However, for the out of plane transverse shear stiffness, a totally different trend can be observed. For a cell angle varying between -50 to -30°, the change in the transverse shear moduli is more significant. These observations can be useful to design hexagonal auxetic structures for a specific loading case, such as torsion or bending. It also worth mentioning that the effect of the variation

of in-plane shear stiffness G_{xy} on the RSPL, which is the objective function of this study, is negligible [45].

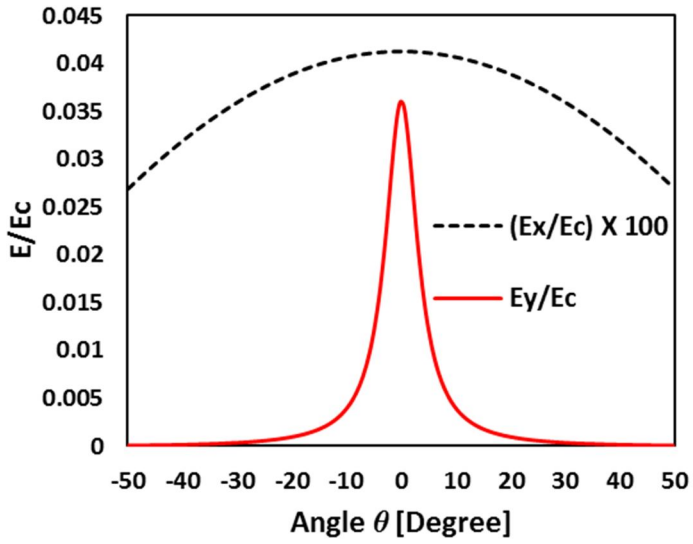

Figure 8: Variation of the in-plane mechanical properties of an auxetic hexagonal honeycomb, cell wall aspect ratio for internal cell angle of -30º is 2.

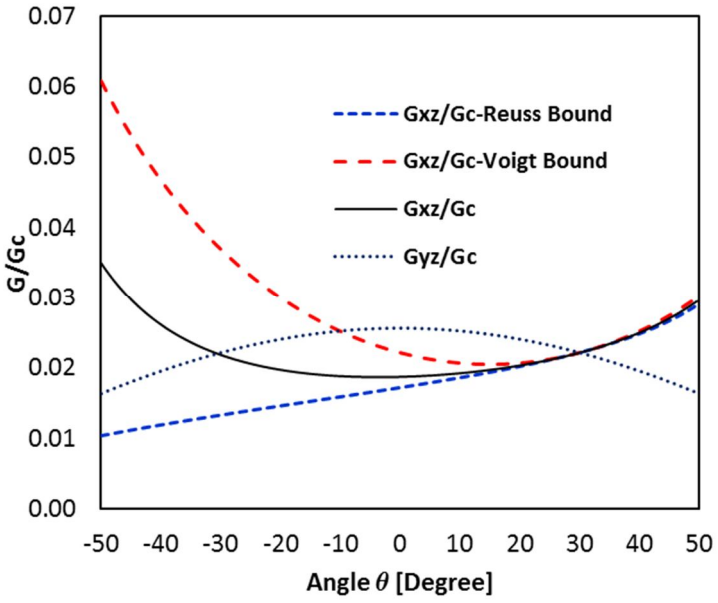

Figure 9: Variation of the out of plane mechanical properties of an auxetic hexagonal honeycomb core, cell wall aspect ratio for internal cell angle of -30º is 2.

3.2.2 Finite Element Modelling of the Hexagonal Sandwich Structure

The modal analysis for the auxetic hexagonal honeycomb sandwich structure with the uniform (constant angle) cell distribution has been performed using the ANSYS Rel. 14.0 commercial FE analysis package.

An exact FE sandwich structure with a core made from 18×30 auxetic hexagonal honeycomb unit cells has been demonstrated in Figure 10. The geometrical parameters of the auxetic hexagonal honeycomb core are listed in Table 2.

Table 2: Geometrical parameters of auxetic hexagonal honeycomb core

h (mm)	l (mm)	t (mm)	b (mm)	θ (degree)
36.95	18.48	1	20	-30

The core is covered with two 960×960×2 mm skins plates. Both core and skins are made of ABS plastic with elastic properties listed in [44].

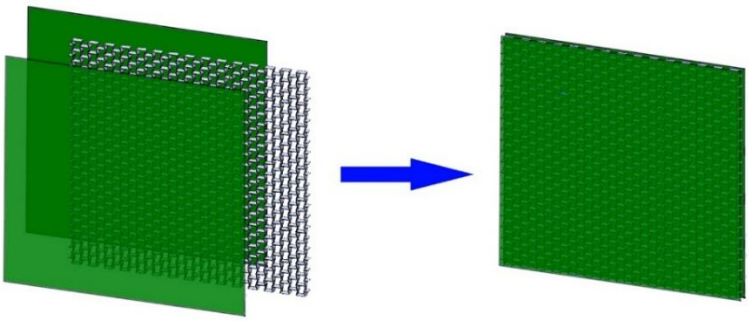

Figure 10: Exact FE layout of the sandwich structure with auxetic hexagonal core

The Unit cell homogenization approach has been previously applied to calculate the vibroacoustic behavior of auxetic structures by Chekkal et al. [43]. To perform the homogenization of the sandwich structure, two solid elements per gauge thickness

have been considered to represent the homogenized core of the auxetic hexagonal honeycomb and the skins have been modeled using shell elements. The mechanical properties of the skin are the same as the one of ABS plastics, while the mechanical properties of the homogenized core can be defined using the compliance matrix [S]. Figure 11 shows a homogenized model of a hexagonal honeycomb structure and an example of a single unit cell, with a core and two skins. The homogenized unit cell is then reproduced along both the x and y directions to make the sandwich structures with overall dimensions mentioned above. To determine the most appropriate element types to represent the homogenized auxetic sandwich structure, a sensitivity analysis with respect to the natural frequency of the full-homogenized model is done[44], [45]. Different element types are considered to model the skin and the core of auxetic sandwich structure, and Shell 63 and Solid 45 elements from the ANSYS Rel. 14.0 commercial code have been considered to model the skin and the core, respectively. A brief introduction about properties of the mentioned element types can be found in Appendix A.

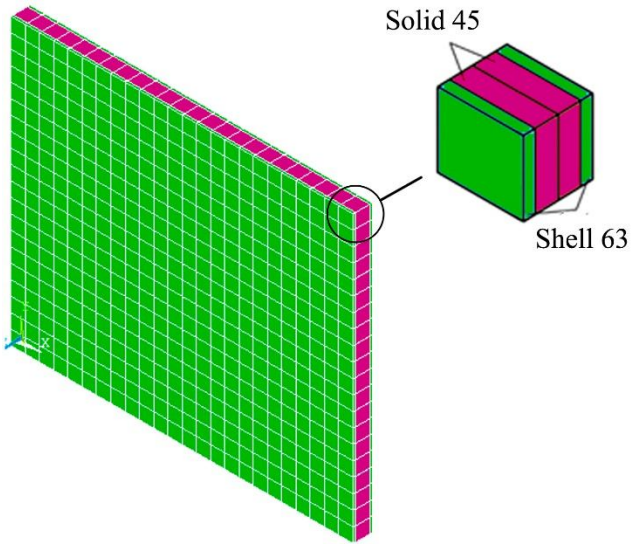

Figure 11: FE model of a homogenized auxetic sandwich structure and a representative unit cell

3.2.3 Model Verification

To verify the validity of the homogenized modeling, a modal analysis has been performed to compare the natural frequencies of the homogenized FE model and the exact FE model, which represents the detailed geometry of the core and the skin of the panel (Figure 10). For the exact FE model both core and skins are represented by SHELL63 elements, with constant elements size of b/4 in the exact FE model [45]. Simply supported boundary conditions (SSBC) are considered for the modal analysis. To apply SSBC the nodes located at the half-plane of the core in both the homogenized and exact FE models are fixed. The total number of elements for the exact FE model was 51721 elements while for the homogenized model this number was decreased to 2304 elements. The Block Lanczos solver has been used to perform the modal analysis. Table 3 shows the result of modal analysis of the auxetic hexagonal honeycomb sandwich structure for both models. Figure 12 shows the first four mode shapes for both models. The first six mode shapes in both homogenized and exact FE model are similar. Moreover, the natural frequencies found by the homogenized model are in good agreement with the ones calculated by the exact FE model. This result confirms that the homogenized model represents an excellent approximation of the exact FE model, especially in frequency range 0-200 Hz.

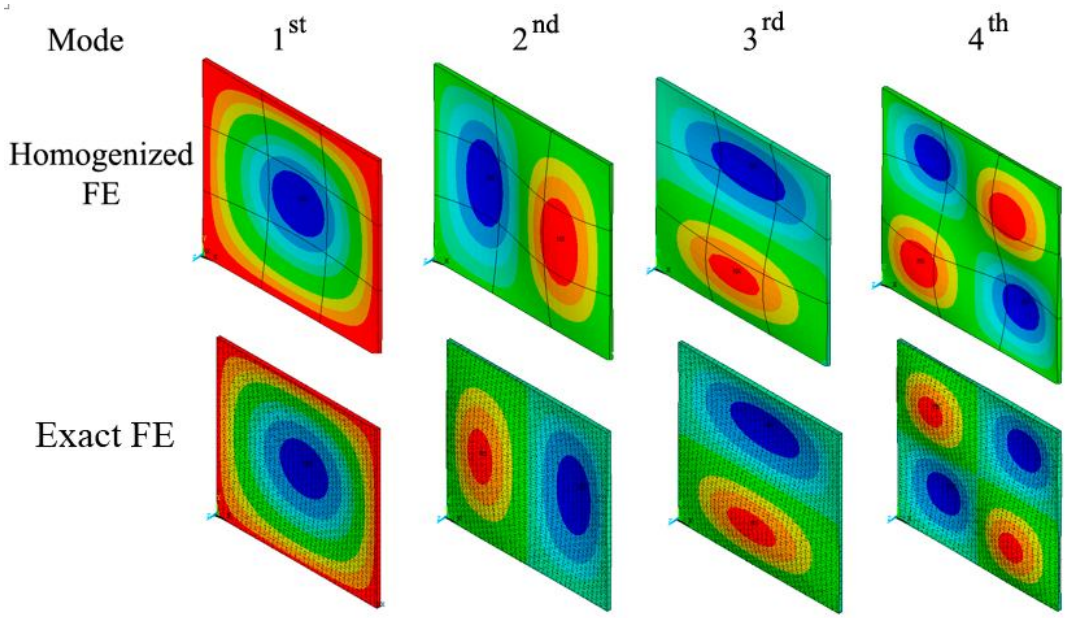

Figure 12: The first four mode shapes for the homogenized FE model and the exact FE model

Table 3: Modal analysis comparison of the homogenized and the exact FE models, case 1

	Model	1st	2nd	3rd	4th	5th	6th
Frequency (Hz)	Homogenized FE	37.84	91.78	94.76	143.90	179.10	183.4
	Exact FE	34.80	83.84	87.31	133.17	160.88	170.9

3.3 Homogenization Modeling of the Anti-tetrachiral Lattices

There have been several pieces of research that aim to predict the mechanical properties of chiral lattices. Chen et al. [22] have used an analytical method to predict the mechanical properties of anti-tetrachiral lattices. In the following calculation of the mechanical properties of these lattices have been proposed.

3.3.1 Mechanical Properties of the Anti-tetrachiral Lattices

An analytical model has been used to calculate the mechanical properties of anti-tetrachiral lattices. Figure 13 shows a typical panel with a Representative Unit Cell (RUC) of the anti-tetrachiral lattice.

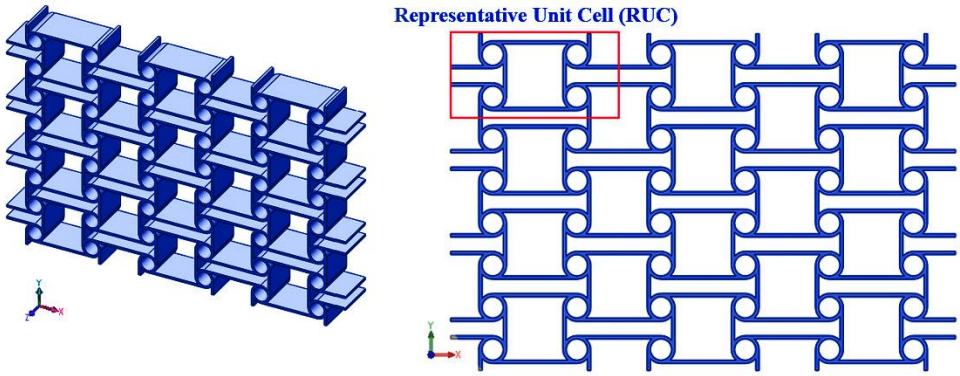

Figure 13: Anti-tetrachiral plate and its representative unit cell

Chen et al. [22] used an analytical approach based on strain energy methods to calculate mechanical properties of the anisotropic anti-tetrachiral lattice. Figure 14 represents the RUC with all its geometrical parameters. The parameters L_x and L_y are ligaments length along the x and y-direction respectively, r is the radius of the node and t_l represents the thickness of the ligaments. Four non-dimensional parameters $\alpha_x = \frac{L_x}{r}$, $\alpha_y = \frac{L_y}{r}$, $\beta = \frac{t_l}{r}$, $\gamma = \frac{b}{r}$ have been defined.

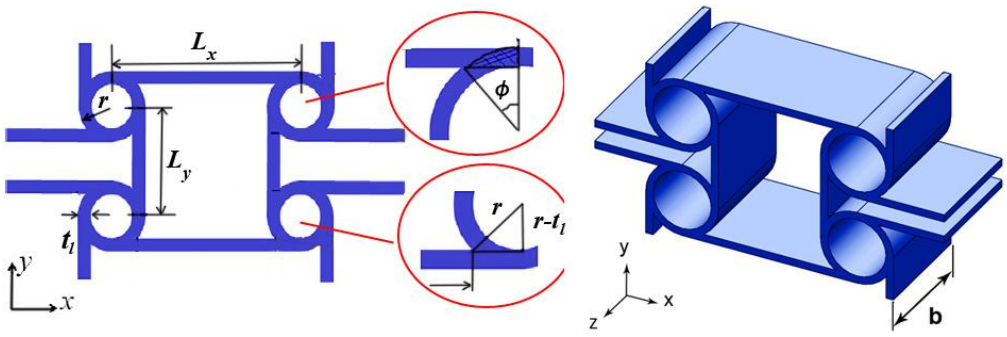

Figure 14: Representative Unit Cell (RUC) and the geometrical parameters

The following equations show the analytical formulation used to represent the in-plane mechanical properties of the anisotropic anti-tetrachiral lattice. The-in plane mechanical properties can be derived as follows:

$$\upsilon_{xy} = -\frac{L_x}{L_y} \tag{13}$$

$$E_x = \frac{E_c \beta^3 \alpha_x}{12(1-\frac{\beta}{2})^2 \alpha_y}\left(\frac{1}{\alpha_x - 2\sqrt{2\beta-\beta^2}} + \frac{1}{\alpha_y - 2\sqrt{2\beta-\beta^2}}\right) \tag{14}$$

$$E_y = \frac{E_c \beta^3 \alpha_y}{12(1-\frac{\beta}{2})^2 \alpha_x}\left(\frac{1}{\alpha_x - 2\sqrt{2\beta-\beta^2}} + \frac{1}{\alpha_y - 2\sqrt{2\beta-\beta^2}}\right) \tag{15}$$

In Equations (14) and (15), E_x and E_y are the elastic moduli along the *x* and *y* directions. When the ligament lengths along the *x* and *y*-directions are equal ($\alpha_x = \alpha_y$), the following formula can be obtained for a transversely isotropic lattice:

$$E_x = E_y = \frac{E_c \beta^3 \alpha}{12(1-\frac{\beta}{2})^2}\left(\frac{1}{\alpha - 2\sqrt{2\beta-\beta^2}}\right) \tag{16}$$

The elastic modulus along the z-direction is represented by the following equation

$$E_z = E_c \beta \frac{[\alpha_x + \alpha_y + \pi(2-\beta)] - 2[\varphi - (1-\beta)\sin\varphi]}{\alpha_x \alpha_y} \tag{17}$$

In which

$$\mathrm{j} = \cos^{-1}(1 - \mathrm{b}) \tag{18}$$

Theoretically, the transverse shear modulus of general honeycomb structures is limited within an upper (Voigt) and a lower (Reuss) bound. Those bounds can be obtained by using the theorems of the minimum potential and minimum complementary energies [22]. The expressions of the upper bounds are the following:

$$G_{xz} \le \frac{\alpha_x + \pi}{\alpha_x \alpha_y} \beta G_c \tag{19}$$

$$G_{yz} \le \frac{\alpha_y + \pi}{\alpha_x \alpha_y} \beta G_c \tag{20}$$

If we consider equal ligament lengths along the x and - directions, i.e. $\alpha_x = \alpha_y$, then it is possible to obtain the upper bound for a transversely isotropic lattice as:

$$G_{xz} = G_{yz} \le \frac{\alpha + \pi}{\alpha^2} \beta G_c \tag{21}$$

Lorato et al. [33] proposed another formula for the calculation of the lower bond for the transversely isotropic lattice when $\alpha_x = \alpha_y$.In which for anti-tetrachiral configuration $k_1 = 0.045$ and $k_2 = 0.67$:

$$G_{xz} = G_{yz} \ge \alpha \frac{k_1}{1 + \alpha k_2} \beta G_c \tag{22}$$

The transverse shear modulus can also be expressed as in [33], in which the coefficient *K* for the anti-tetrachiral lattice is equal to 1.57:

$$G = G_{low} + \frac{K}{\gamma}(G_{up} - G_{low}) \tag{23}$$

The geometry of the exact detailed ATG plate configuration is replaced by an equivalent orthotropic material using a compliance matrix [S] defined in Equation (12), in which the engineering constants E_x, E_y, E_z, G_{xy} and G_{xz} can be derived from above formulae. The out-of-plane Poisson's ratios υ_{xz} and υ_{yz} are assumed to be near zero, consistently with the assumptions of the Cellular Material Theory [9], [44]. Similarly, the other transverse Poisson's ratios are assumed to satisfy the relation $\upsilon_{zx} = \upsilon_{zy} \approx \upsilon_c$ where υ_c is the Poisson's ratio of the core material [9], [44]. The transverse shear modulus (G_{xy}) of the anti-tetrachiral cell can be found from the formula $G_{xy} = \frac{E_x}{2(1+\upsilon_{xy})}$. This equation cannot be defined for υ_{xy} = -1. Therefore, as indicated by Alderson et al. in anti-tetrachiral systems [7], [28], the in-plane Poisson's ratio derived by FE modeling and experiment analyses can be considered equal to -

0.98. Figure 15 shows the sensitivity of the in-plane modulus along the x-direction with respect to the radius of the unit cell. The Young's modulus has been normalized against the tensile modulus of the core material, E_C, which is represented by acrylonitrile butadiene styrene (ABS) [44]. As the radius of the nodes increases, the longitudinal stiffness has a decrement proportional to r^{-1}, as it can be noticed by inspecting Equations (14-16).

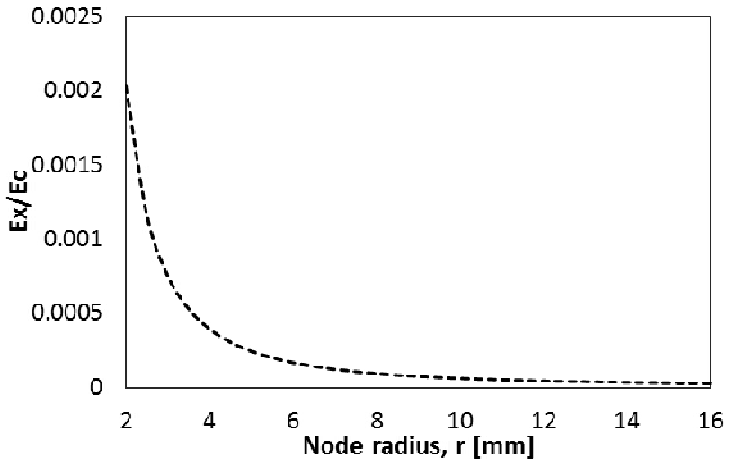

Figure 15: In-plane Young's modulus *Ex* ratio with respect to ATG unit cell radius with $L_x=L_y=40$ *mm*, $t_1=1$*mm* and $b=20$*mm*

Figure 16 shows the out-of-plane stiffness E_z is linearly dependent on the radius of the nodes *r*, as expected when considering that the out-of-plane Young's modulus scales as the density of the honeycomb structure [9], [22].

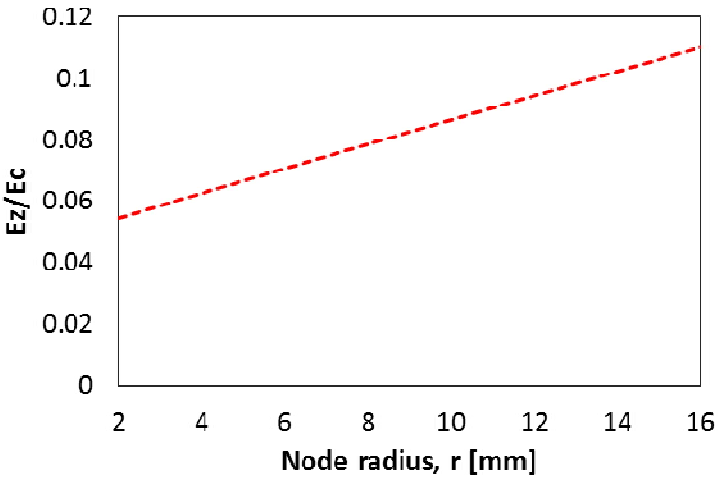

Figure 16: Out of plane stiffness E_z with respect to the radius of the unit cell r

Figure 17 demonstrates the variation of out-of-plane transverse shear stiffness G_{xz} or G_{yz} with respect to the r. in case of a transverse isotropic lattice. For increasing values of the radius of the nodes, the out-of-plane shear modulus has a nonlinear behavior, with an initial minima and a steep increase at higher values of r when considering the numerical values of the ligament lengths and thickness considered.

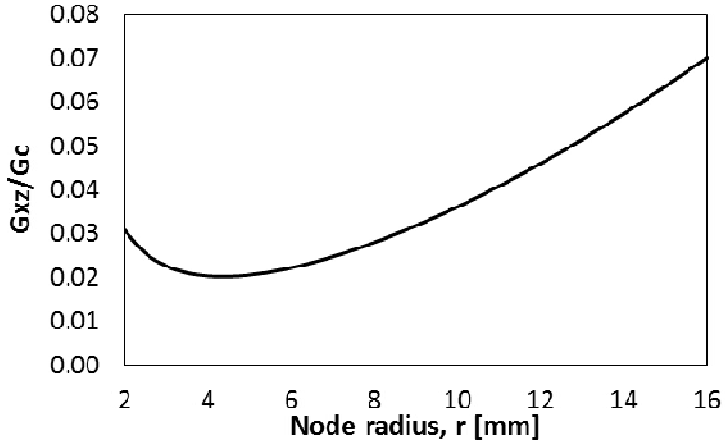

Figure 17: Variation of out of plane ATG transverse shear stiffness G_{xz} or G_{yz}

3.3.2 Finite Element Modelling of the Anti-Tetrachiral Sandwich Structure

Figure 18 shows a full scale detailed model of the sandwich structure with a core made of 12×12 auxetic anti-terachiral cell and the proposed homogenized model. As it has

mentioned before the exact FE model can be replaced with a homogenized model in which an orthotropic material is used to model core of the sandwich structure. The geometrical parameters of the core are listed in Table 4.

Table 4: Geometrical parameters of anti-tetrachiral core

r (mm)	L_x(mm)	L_y(mm)	t_l (mm)	b (mm)
8	40	40	1	20

The anti-tetrachiral core is covered with two 960×960×2 mm skins plates. Both core and skins are made of ABS plastic with elastic properties listed in [44].

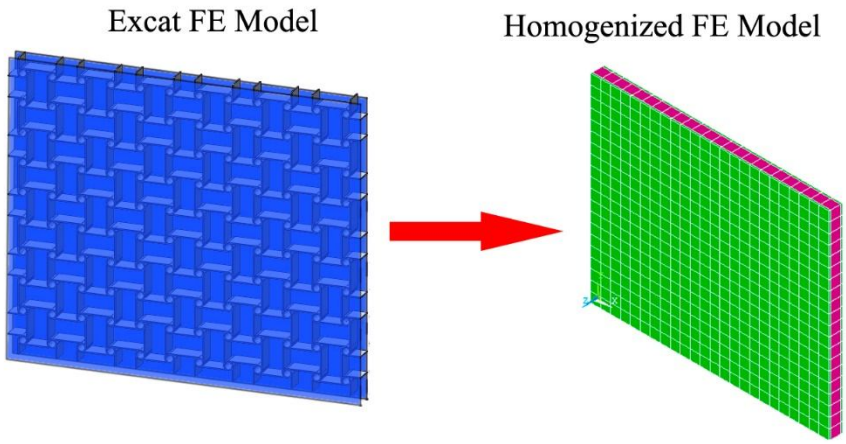

Figure 18: Exact FE layout of the sandwich structure with anti-tetrachiral core and the homogenized model

Chekal et al. [43] have previously used the unit cell homogenization approach to analyse the vibroacoustic behavior of auxetic structures. In the homogenized model, two solid elements have been considered to represent the homogenized anti-tetrachiral core while the skins have been modeled using shell elements. The mechanical properties of the skin are the same as the one of ABS plastics, while the mechanical properties of the homogenized core can be defined using the compliance matrix [S].

In Figure 19 a homogenized unit cell having a core and two skins is demonstrated. The homogenized unit cell is then reproduced along both the x and-y directions to make the sandwich structures with overall dimensions mentioned above. The element selection for the core and the skins is performed in the same manner which has been carried out for the auxetic hexagonal honeycomb structure.

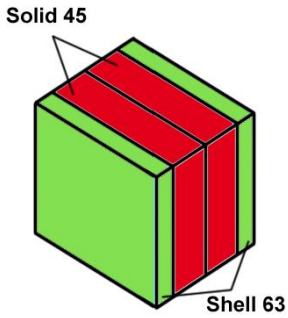

Figure 19: FE model of a homogenized auxetic sandwich structure unit cell

3.3.3 Model Verification

To verify the validity of the homogenized modeling, a modals analysis has been performed to compare the natural frequencies of the exact FE homogenized model and the exact FE model. Table 5 shows the natural frequencies of the homogenized model and the exact FE model, which represents the detailed geometry of the core and the skin of the panel. Both the core cells and the skins are represented by SHELL63 elements, with constant elements size of b/4 in the exact FE model. Simply supported boundary conditions (SSBC) are considered for the modal analysis. The total number of elements for the exact FE model was 49728 elements while for the homogenized model this number was decreased to 2304 elements. The Block Lanczos solver has been used to perform the modal analysis. Table 5 shows the result of modal analysis of the auxetic anti-tetrachiral honeycomb sandwich structure for both models. The first six mode shapes in both homogenized and exact FE model are similar. Moreover, the

natural frequencies found by the homogenized model are in good agreement with the ones calculated by the exact FE model. This result confirms that the homogenized model represents an excellent approximation of the exact FE model, especially in frequency range 0-200 Hz.

Table 5: Modal Analysis comparison of the homogenized and the exact FE models, case 2

	Model	1st	2nd	3rd	4th	5th	6th
Frequency (Hz)	Homogenized FE	39.10	95.44	95.44	146.05	182.53	182.53
	Exact FE	36.19	88.65	88.65	136.96	170.58	170.58

Once the homogenized model has been validated, the analysis of the radiated sound power can be performed. In the next chapter, the analysis of radiated sound power for sandwich structures with auxetic hexagonal honeycomb core and anti-tetrachiral core has been carried out.

Chapter 4

STRUCTURAL ACOUSTIC OF THE SANDWICH STRUCTURE

4.1 Introduction

This chapter provides theoretical analysis on the structural acoustics. This analysis is required for the optimization calculations presented in the following chapters. In section 4.2 the analytical formula on the structural acoustic have been proposed while section 4.3 sheds light on the finite element modeling of the sandwich structure under different loading conditions.

4.2 Radiated Sound Power

The level of radiated sound power, $L_s(f)$, has been used as a reliable measure to determine the emitted noise emitted from structures [69]. Radiated sound power level (RSPL) or sound power level for short can be defined as a function of frequency:

$$L_s(f) = 10 \times \log \frac{P(f)}{P_0} dB \tag{24}$$

Where, $P(f)$ is the radiated sound power, P_0 is a standardized reference value which is equal to 10^{-12} W and f is the frequency in Hz. $P(f)$ also can be defined as [69]:

$$P(f) = \frac{1}{2} \rho_a c_a S \overline{v_{\perp rms}^2}(f) \sigma(f) \tag{25}$$

Where, $c_a (m.s^{-1})$ and $\rho_a (kg.m^{-3})$ are the speed of sound in the surrounding fluid (air in this case) and the density, respectively, S is the area of the surface from which sound

is radiated (the surface of the sandwich structure), $\sigma(f)$ is the radiation efficiency and $v^2_{\perp rms}(f)$ is the mean squared normal velocity of the surface which is averaged over the sound radiating surface.

There are two ways to obtain the rms velocity vector, $v_{rmsi}(f)$, at point *i* on the sound radiating surface. First method is to do an experimental measurement using accelerometers or a laser vibrometer, while the second method is a numerical method using a dynamic FE analysis. Either way, the normal component of the rms velocity vector, $v_{\perp rmsi}(f)$, is then calculated by

$$v_{\perp rmsi}(f) = v_{rmsi}(f) \cdot n_i \tag{26}$$

Where, n_i is the unit normal vector on that particular surface point.

Once the $v_{\perp rmsi}(f)$ at all the nodal points of meshed structure's surface is known, the mean squared rms normal velocity can be averaged over the radiating surface as follows:

$$\overline{v^2_{\perp rmsi}(f)} = \frac{1}{n_n} \sum_{i=1}^{n_n} v^2_{\perp rmsi}(f) \tag{27}$$

Where, n_n is the number of the measurement points or the finite element nodes on the radiating surface of the structure.

Therefore, the radiated sound power level, L_S, can be calculated using the above formulae.

It is worth mentioning that in the present research the velocity vectors, $v_{\perp rmsi}(f)$, are only calculated by means of the FEM using a modal superposition technique, which is admissible for lightly damped structures. This means that each FE analysis consists of the two consecutive steps: The first step is a numerical modal analysis, which

determines the natural frequencies and the mode shapes of the structure. In the second step, the velocity vectors, $v_{\perp rmsi}(f)$, are obtained by superposition of the previously computed mode shapes using scalar mode participation factors [1]. The mode participation factors can be regarded as weighting factors, which show the proportions of each mode occurring [1]. The numerical modal analysis in the first step ensures that all natural frequencies and mode shapes in the frequency band of the interest are automatically taken into account and none can be missed when the vibrational response of the structure subject to some force excitation is calculated in the second step.

Moreover, as it has been indicated by Fritze et al. [70] that considering the solution of the fluid part of the structural acoustic for the exterior acoustic problems is significantly time-consuming and it appears as a bottleneck in the optimization process. To avoid solving the acoustic boundary value problem related to the calculation of the radiated sound power L_s, an acceptable approximation is the use of the equivalent radiated sound power (ERP) [69]. In this case, the radiation efficiency is considered equal to 1.0. The ERP will not cause any local acoustic effect, as in all Finite element simulations same radiation efficiency of $\sigma = 1$ is adopted. The ERP will therefore usually overestimate the sound radiation, however, it will provide an adequate approximation for the structure-induced acoustical problems, especially as an upper bound estimation [65], [70].

Since acoustic power is determined by the surface velocity, one alternative and less computationally expensive objective function, is to only consider the vibrational efficiency of the structure as expressed by the mean square normal velocity [65]. The radiated sound power level, L_S, in Equation 24 is a function of the frequency and it

includes a frequency spectrum. To obtain a single global measure of the vibrational behavior of the structure in a given frequency range, the root mean square level of the structure-borne sound over that frequency band, known hereafter as RMLS, is calculated as follows:

$$RMSL = \sqrt{\frac{\int_{f_{\min}}^{f_{\max}} Ls^2(f)df}{f_{\max} - f_{\min}}} dB \tag{28}$$

In which, f_{max} and f_{min} are upper and lower bounds of the frequency range. RMSL can be considered a special quantity characterizing the vibrational energy contained in the given frequency range. It serves as the objective function of the optimization problem in this research.

4.3. Finite Element Modeling

As it was mentioned in Chapter 3, once the homogenized model of the sandwich is validated by the modal analysis results, the analysis of the radiated sound power can be performed. The sandwich structure is modeled by Shell 63 elements representing the skin and Solid 45 elements modeling the core. The boundary conditions is a simply supported boundary condition and it is applied simply by fixing all the nodes located on the on the mid-plane of the core. The excitation applied by harmonic pressure loads. There are two different loading conditions applied on the sandwich structure to excite different modes of the model.

Figure 20 shows loading case ‘a’ which consists of three local pressure excitations, while in loading case ‘b’, (Figure 21) a full pressure exerted on the whole external skin surface. The magnitude of pressure is 2.5 kPa and it has been applied to the elements in the z-direction with a frequency range of 0-200 Hz.

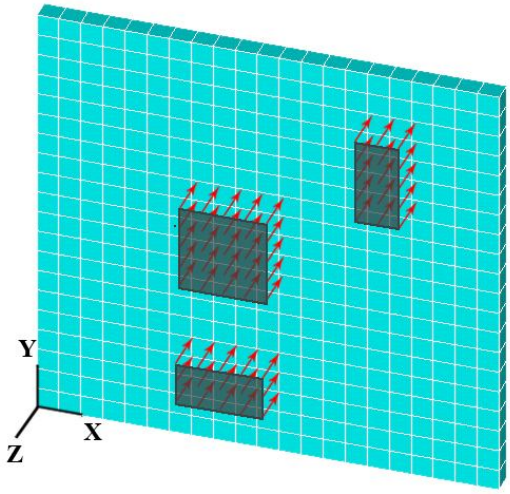

Figure 20: Loading case ‘a’, local pressure excitation

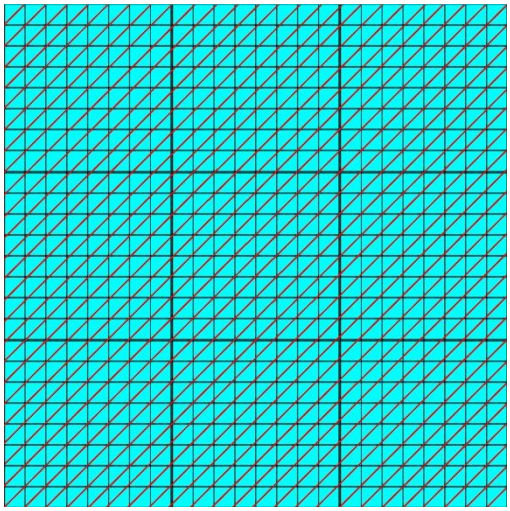

Figure 21: Loading Case ‘b’, full load pressure excitation

Once the loading excitation has been defined, the harmonic analysis in ANSYS software will be performed to obtain radiated sound power level and RMSL. In order to do that a macro code has been developed to generate the geometry of the sandwich structure, define material properties and perform the modal and the harmonic analysis. This macro code includes Equations (24-28). Once the harmonic analysis is done, the rms normal velocity in z-direction, $v_{\perp rmsi}(f)$, will be found for all the nodes on the radiating surface. Then, using Equation 27 the averaged mean squared rms normal

velocity can be found. Next, Equation 24 and 28 will be employed to define the radiated sound power level as a function of frequency and RMSL respectively.

The results for the RSPL and RMSL for the sandwich structures with auxetic hexagonal honeycomb core and anti-tetrachiral core will be illustrated in detail in chapter 5 and 6. The overall flow chart of the modeling and optimization of the auxetic sandwich structures is shown in Figure 22.

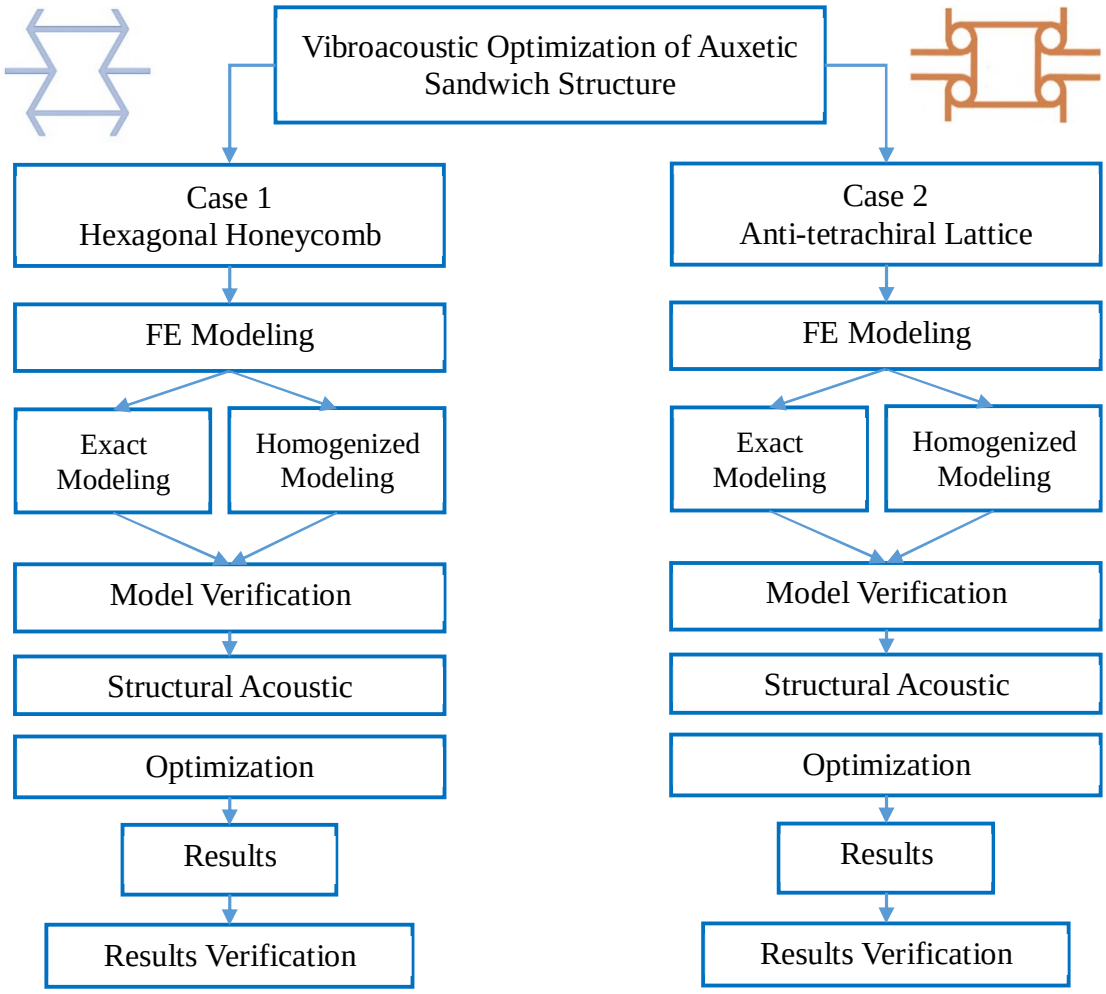

Figure 22: The Vibroacoustic optimization flowchart

Chapter 5

VIBROACOUSTIC OPTIMIZATION OF THE 2D GRADIENT HEXAGONAL HONEYCOMB SANDWICH STRUCTURE

5.1 Introduction

This chapter describes the vibroacoustic behavior of sandwich structure with hexagonal honeycomb cores. First, in section 5.2 a comparison between sandwich structures and simple plates in terms of vibroacoustic behavior is shown. Next, the variation of the RMSL with respect to the change of the internal cell angle on the RMSL is demonstrated. Then, the effect of gradient topology of the core on the RMSL is investigated in section 5.3. In section 5.4, the RMSL optimization of the 2D gradient hexagonal honeycomb sandwich structure is studied. In section 5.5, the thickness optimization of these sandwich structure has been evaluated and finally in section 5.6 the normalized RSPL is discussed.

5.2 RMSL Comparison between Sandwich structure and a Simple Plate

First, to show that the sandwich structures perform better than simple plates with respect to vibroacoustic behavior, three assorted configurations have been considered and the RMSL have been calculated for each of them. The first configuration is a $996 \times 960 \times 20$ mm sandwich structure with a uniform (non-gradient) conventional hexagonal honeycomb core with an internal angle of 30. The second configuration is

represented by a simple plate with the same mass of the previous configuration, i.e. 5.221 kg. To possess the same mass the thickness of the plate is however reduced and the dimension is $996 \times 960 \times 5.25$ mm. The third configuration is a simple plate with the same dimensions of the first configuration. In this configuration, the core and the skin material are similar. As this plate is not a sandwich structure the mass increases more than 3 times. The RMSL for all these configurations under the loading case 'a' shown in Figure 20 is illustrated in Table 6.

Table 6: RMSL and mass for the sandwich structure and simple plate

Configuration No.	Dimension [mm]	Core properties	Mass [kg]	RMSL [dB]
1	$996 \times 960 \times 20$	Core is a uniform conventional hexagonal topology with constant angle of 30^o	5.221	127.77
2	$996 \times 960 \times 5.25$	Core is filled with the same ABS material	5.221	137.65
3	$996 \times 960 \times 20$	Core is filled with the same ABS material	19.889	118.45

The first configuration has a noticeably lower RMSL compared to the second configuration, which is a simple non-sandwich structure. The reason behind the lower RMSL is the increased flexural properties of the sandwich structure compared to the simple plate. This higher flexural properties of the sandwich structure is caused by its increased thickness compared to the simple plate. On the other hand, the third configuration shows a significant reduction in RMSL. This reduction in RMSL happens as in this case, the thickness of the plate is same as the sandwich structure and

the core is filled with the same ABS material. However, this reduction in RMSL is accompanied by a mass increase of 300%.

In the next step, the change of the RMSL with respect to the variation of core internal angle for a non-gradient sandwich structure is shown in Figure 23. The RMSL in the sandwich structures with negative core angles (auxetic core) is generally lower than the RMSL in sandwich structures with positive core angles. This is because of the auxetic cores generally, have higher out of plane bending stiffness provided by the transverse shear G_{xz} (see Figure 9). The small discontinuity for $\theta=0^o$ is due to the different interpolation coefficients used for the transverse shear G_{xz} for positive and negative internal cell angle which has been mentioned in Equation 11. It can also be noted that the sandwich structure with a core angle of -50^o shows minimum RMSL.

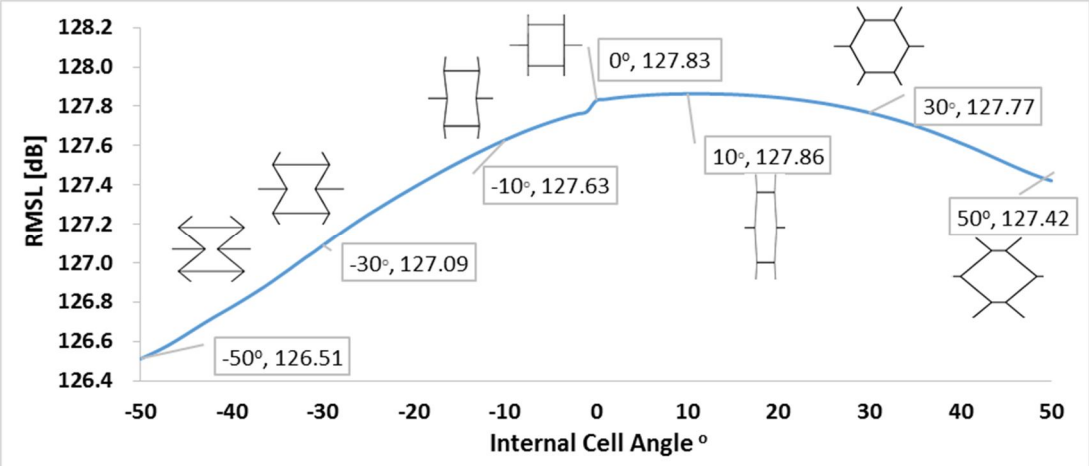

Figure 23: Change of the RMSL with respect to variation of core angle for a non-gradient sandwich structure

In the next section, a gradient topology for the core of the sandwich structure will be proposed and the effect of this topology on the vibroacoustic behavior of the sandwich structures will be investigated.

5.3 Gradient Topology

The core geometry of the sandwich structure shown in Table 6 was a uniform core geometry. In another word, the core cellular structure was made of cells having the same geometry in any part of the structure. It is, however, possible to produce this cellular structure with a gradient configuration. The configuration in this gradient topology is made of a continuous distribution of unit cells with compatible geometry, but having a single variable parameter like the internal cell angle [45]. In gradient configuration, using a gradient cellular structure will lead to a varying distribution of stiffness and deformation. Therefore, different mechanical properties can be achieved in different areas of the structure. Having desired mechanical properties in the various regions of the core will lead to having better vibroacoustical behavior [45].

Figure 24 shows an example of a 2D gradient hexagonal cellular configuration. As it can be seen in this figure the core geometries in different regions are different. The 2D gradient core consists of nine different regions with nine different internal angle θ.

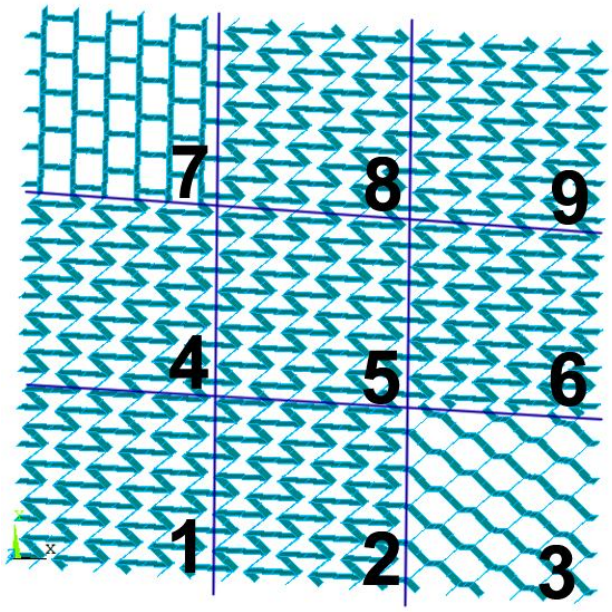

Figure 24: 2D gradient hexagonal honeycomb core having nine different regions

Figure 25 demonstrates a gradient geometry for a unit cell. To generate the 2D gradient core configuration, the unit cells with different internal angle θ have been assembled next to each other. The length L_1 and the position of six points 1-6 shown in the figure are fixed. Therefore, these unit cells can be simply assembled next to each other in x and y-direction to form the 2D gradient core. The geometry and mechanical properties of the unit cells will change with a change in angle θ while the length L_1 and points 1-6 are fixed. The formula proposed in Chapter 3 can be used to determine the mechanical properties in each region. The geometrical parameters of the base line auxetic hexagonal unit cell have been shown in Table 2.

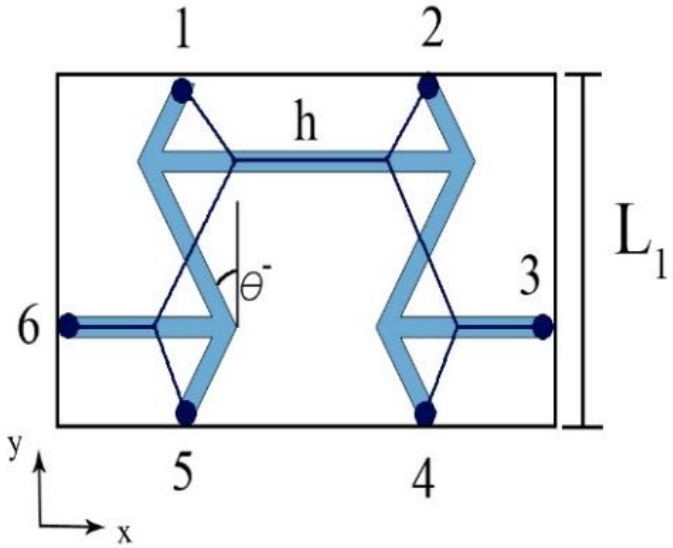

Figure 25: Gradient geometry for a unit cell with changing angles and fixed points 1-6

Figure 26 shows the distribution of the homogenized auxetic hexagonal unit cells for the 2D gradient topology for the loading cases ‘a’ and ‘b’. The nine different regions with nine different angles ($\theta_1, \theta_2, \theta_3, \theta_4, \theta_5, \theta_6, \theta_7, \theta_8, \theta_9$) are assembled next to each other to form the whole sandwich structure. Each region is shown with a distinct

color. The main objective of the optimization problem is to minimize the RMSL by modifying the geometry of the model in each of these 9 regions.

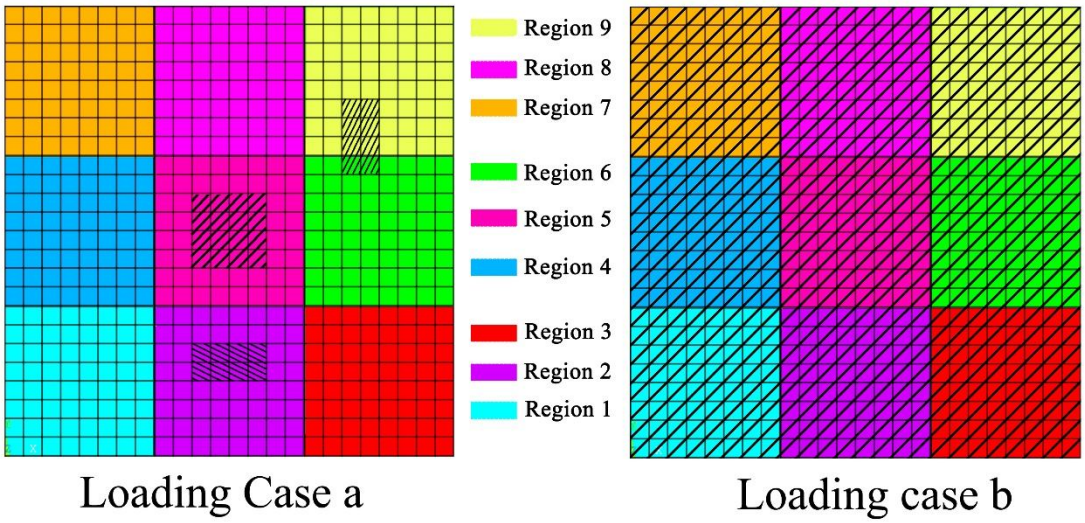

Figure 26: Different external pressure loadings (dashed areas) on the homogenized finite element model of 2D gradient sandwich structure

In the following section, the minimization of the radiated sound power level for the sandwich structures with 2D gradient core will be presented.

5.4 Optimization of the 2D Gradient Core

The minimization process of RSPL over the frequency range of 0 to 200 Hz is discussed in this section. The objective function for the optimization process is the root mean square level of radiated sound power level (RMSL) of sandwich structure. The design variables of this optimization problem are the angles of the unit cells in the different regions. The general optimization problem is, then defined as:

$$\begin{aligned} &\text{Minimize RMSL}\left(\theta_1,\theta_2,\theta_3,\theta_4,\theta_5,\theta_6,\theta_7,\theta_8,\theta_9\right) \\ &\text{S. t.} -50 \le \theta_1,\theta_2,\theta_3,\theta_4,\theta_5,\theta_6,\theta_7,\theta_8,\theta_9 \le 50 \end{aligned} \tag{29}$$

To do the optimization process two different optimization methods have been considered. The Genetic Algorithm optimization method (GA) and the Method of Moving Asymptotes (MMA) [59], [66].

5.4.1 GA Optimization

Genetic algorithm has been widely used in topology optimization problems. GA optimization method which was first formulated by Holland [71], is a probabilistic optimization method that is based on natural biological evolution. GA is consist of an iterative procedure including four main steps [72], [73]which are:

1- Creation of an initial random population,

2- Performance evaluation of each individual using the fitness function,

3- Selecting individuals to reproduce the new population, applying GA operators, i.e. crossover and mutation

4- Repeating steps 2–3 until a termination criterion is reached.

In this section, GA optimization technique is used to minimize the radiated sound from a sandwich structure. The design variables in the optimization process are the internal cell angles in the different regions of the 2D gradient sandwich structure. The 2D gradient sandwich structure has been divided into nine different regions with nine different angles $\{\theta_1, \theta_2, \theta_3, \theta_4, \theta_5, \theta_6, \theta_7, \theta_8, \theta_9\}^T$. The materials considered for the skin plate and the core are equal (ABS plastics). A fixed value of 20 mm is considered for the core thickness, while the skin thickness is 2 mm. The optimization process has been performed using genetic algorithm optimization method. A custom script has been set up in MATLAB environment. It will store nine design variables in a text file and call the Finite Element ANSYS batch file. The ANSYS software reads the text file as an input and generates the gradient homogenized model. Then, it will mesh the

sandwich structure. The element size for the homogenized FE model in the ANSYS software is 40 mm. In the next step, the ANSYS software performs the modal analysis using Block Lanczos method and the harmonic analysis using a mode superposition method. The objective function (RMSL or root mean square of the radiated sound power level) is calculated inside the FE script at each iteration. This objective function will be stored in a text file and in the next iteration, it will serve as an input for MATLAB. This loop continues until the convergence occurs. Figure 27 shows the flowchart of the optimization process and the interactive link between MATLAB and ANSYS software. The MATLAB codes for integrating MATLAB and ANSYS, calculating the objective function and the codes for Genetic Algorithm optimization can be found in Appendix B.

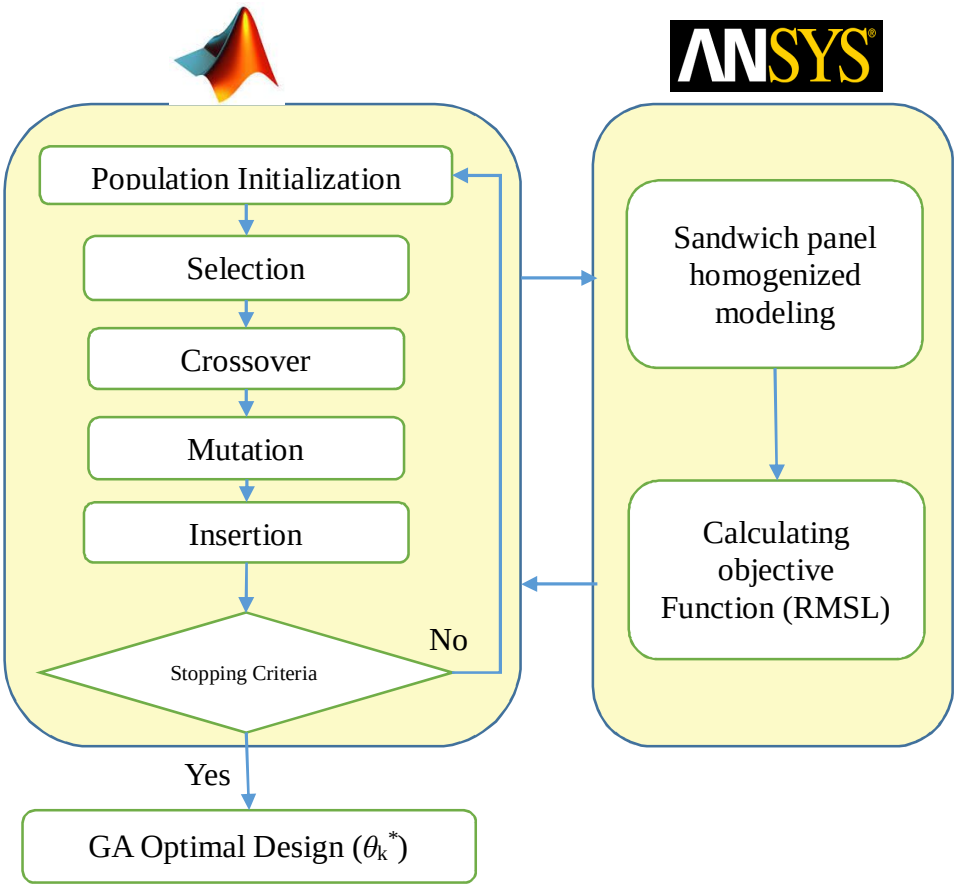

Figure 27: The flowchart of the GA optimization process

As mentioned before, the problem is described by nine design variables. Therefore, selecting a proper population size is a challenge. In order to do that a sensitivity analysis on the order of population size has been performed and the initial population size of 50 is considered. For a better scoping of the feasible design envelope of this optimization problem, the first generation of the genetic algorithm has been created by using a Latin hypercube sampling (LHS) method. Figure 28 shows the plot matrix of the LHS design and the related objective function. The RMSL is calculated for loading case ‘a’.

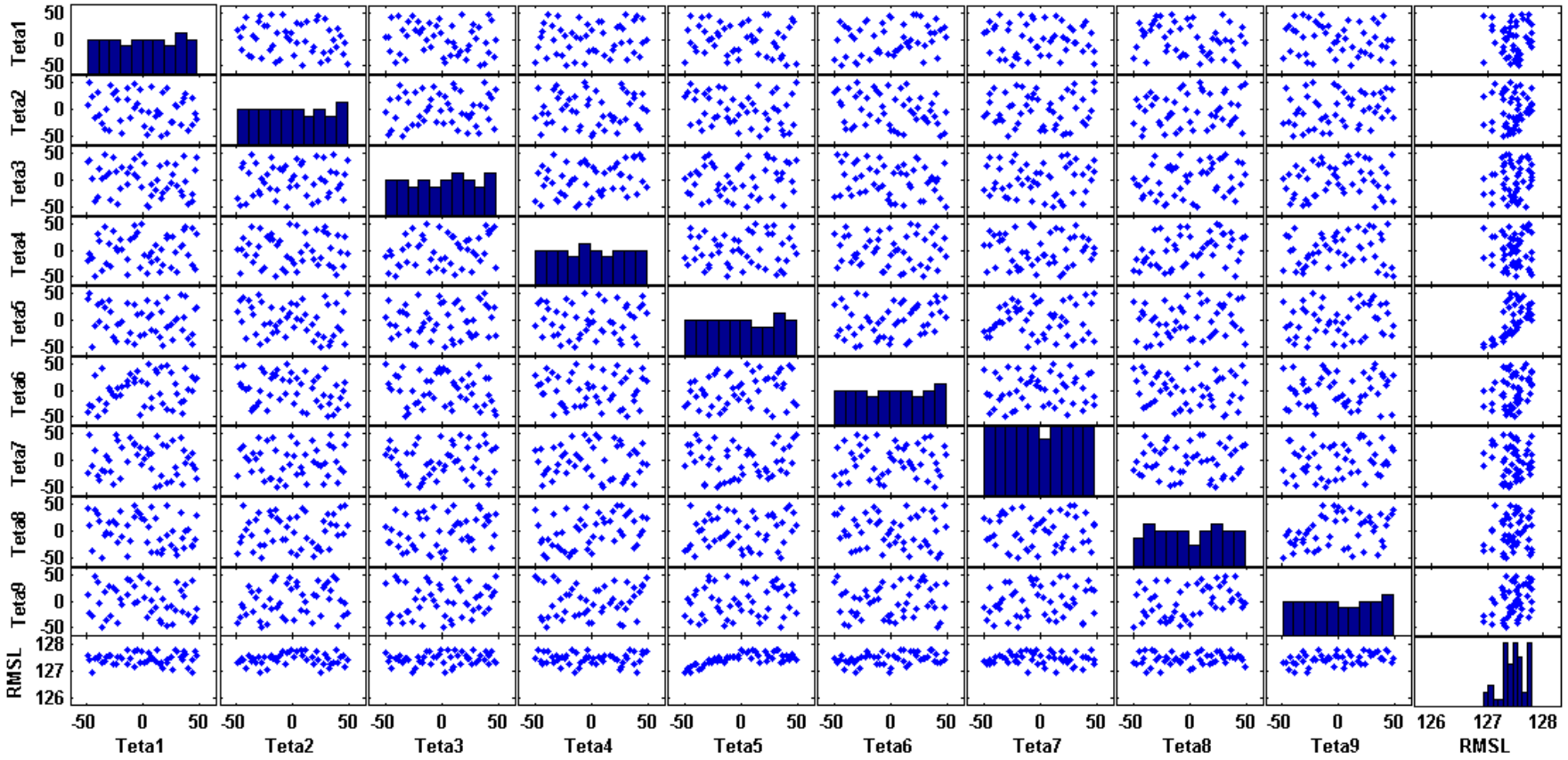

Figure 28: Plot matrix of Latin Hypercube Sampling for the GA initial population

As it is shown in the figure the design variables created by LHS method are evenly distributed in the angles ranging between -50º and 50º. The tenth row and column show the RMSL which is the objective function of this optimization problem. It can be observed that in the regions that the internal cell angle is closer to -50º the RMSL is lower. This finding has been previously observed in

In the next step, the change of the RMSL with respect to the variation of core internal angle for a non-gradient sandwich structure is shown in Figure 23. The RMSL in the sandwich structures with negative core angles (auxetic core) is generally lower than the RMSL in sandwich structures with positive core angles. This is because of the auxetic cores generally, have higher out of plane bending stiffness provided by the transverse shear G_{xz} (see Figure 9). The small discontinuity for $\theta=0^o$ is due to the different interpolation coefficients used for the transverse shear G_{xz} for positive and negative internal cell angle which has been mentioned in Equation 11. It can also be noted that the sandwich structure with a core angle of -50º shows minimum RMSL.

as well. This trend can be seen more specifically in region No. 5 in which it is clear that an increase in internal cell angle, θ_5, will lead to an increase in RMSL.

After having the initial population created by LHS design method, the objective function is then minimized over 100 generations. The crossover probability is 0.8 (must be a number ≤ 1) and the mutation rate is 0.2 (must be a number ≤ 1). Figure 29 and Figure 30 show the variation of the best and the average of the objective function at each generation for the loading cases ‘a’ and ‘b’. For the two cases, convergence is observed after about 80 generations. Each function evaluation takes

about 4.5 CPU seconds on a 2.6 GHz Intel® Core™ i5 processor with 4 GB of RAM operating on a Windows 7 system. The total computation time using the GA method was about 6 hrs. and 15 minutes.

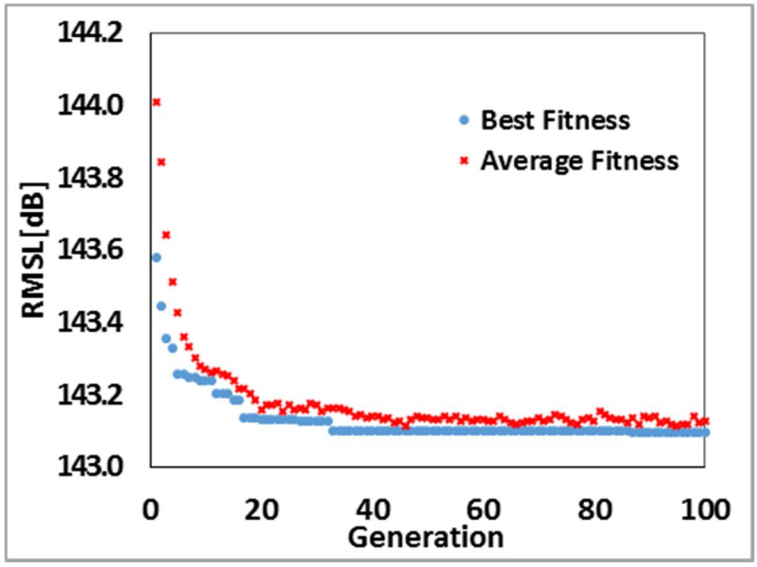

Figure 29: Variation of RMSL per generation during the GA optimization for loading cases ‘a’

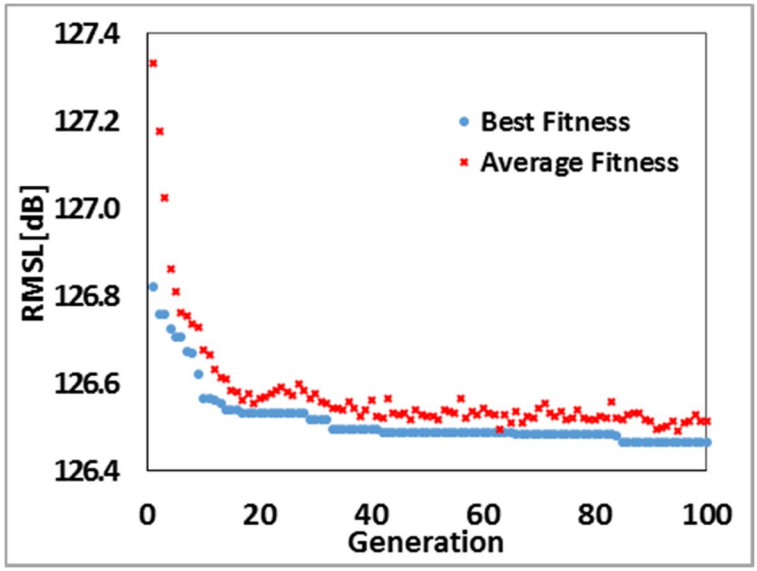

Figure 30: Variation of RMSL per generation during the GA optimization for loading cases ‘b’

5.4.2 MMA Optimization

The other method evaluated in this study for optimization purposes is the Method of Moving Asymptotes (MMA) [59], [66]. In each iteration of the MMA, the objective function is approximated with a strictly convex sub-problem. The generation of these sub-problems is controlled by the moving asymptotes, which may both stabilize and speed up the convergence of the general process [66]. For the first iteration, an initial guess of the design variables, θ_k, is required. Then using the gradient information of the current iteration point (the initial guess), the objective function will be approximated. For the next iterations, this approximation is based not only on gradient information at the current iteration point but also implicitly on information from previous iteration points. The sub-problem is solved and the unique optimal solution becomes the next iteration point. Then a new sub-problem is generated and this procedure continues until a previously defined convergence criteria occurs. The initial guess of the design variables in this research for both loading cases is considered to be

$$\theta_k = \left\{-30^\circ, -30^\circ, -30^\circ, -30^\circ, -30^\circ, -30^\circ, -30^\circ, -30^\circ, -30^\circ\right\}$$

The change of the objective function per iteration for the two loading cases are demonstrated in Figure 31 and Figure 32. It can be seen in both figures that the convergence observed after 8 iterations in this case. It should, however, be mentioned that, as the MMA is a gradient-based method, each iteration includes in this case 18 function evaluations (sub-iterations). Nevertheless, the MMA features a decrease in computation time to 27 minutes.

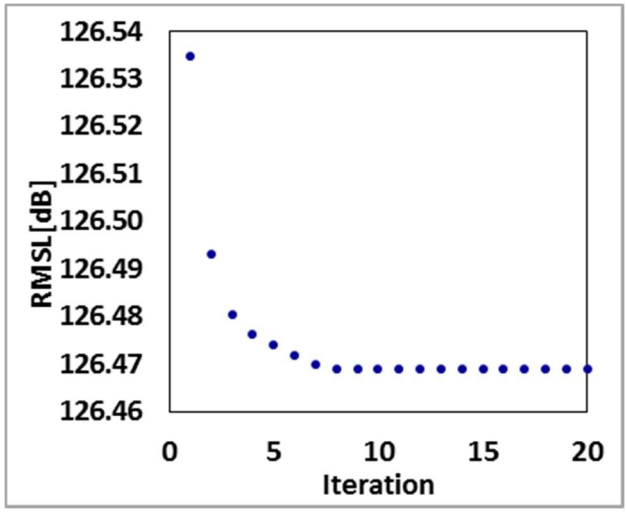

Figure 31: Variation of RMSL per iteration in MMA optimization method, loading cases ‘a’

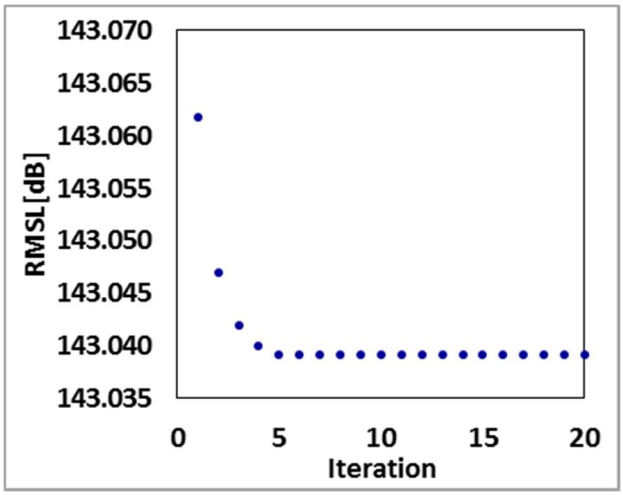

Figure 32: Variation of RMSL per iteration in MMA optimization method, loading cases ‘b’

5.4.3 Hybrid GA-MMA Optimization

To exploit the advantages of both the GA and MMA methods, a hybrid GA-MMA optimization technique is used. In order to do that, the optimal result of the GA optimization has been used as an initial guess for the MMA method. The result of this hybrid optimization shows a slight decrease of the final value of the objective function for the loading case ‘a’. In the case of loading ‘b’ the results of the hybrid and MMA optimizations are alike.

5.5 Optimization Results

In this section, the base line configuration and all optimal configurations of the hexagonal honeycomb sandwich structure have been compared. The base line configuration is a sandwich structure with a total dimensions of $996 \times 960 \times 20$ mm. The core of this sandwich structure consists of 18×30 auxetic hexagonal unit cells with a negative internal angle of $\theta = -30^{\circ}$. The core is covered with two 960×960×2 mm skins plates. Both core and skins are made of ABS plastic with elastic properties listed in [44]. The geometrical parameters of the model are given in Table 2. All the optimized configurations have the same dimensions, material properties and geometrical parameters as the base line configuration. The only difference is that they have different internal cell angles, $\{\theta_1, \theta_2, \theta_3, \theta_4, \theta_5, \theta_6, \theta_7, \theta_8, \theta_9\}$, in different regions of the core.

5.5.1 RMSL Optimization Results

Table 7 and Table 8 show the geometry, optimization variables and total mass of the sandwich panel for the base line and optimal configurations. Table 7 shows that for the load case 'a' the GA reduced the root mean square of sound power level to 126.50 dB, the MMA reduced the objective function to 126.47 dB, while the hybrid GA-MMA gave a final very slight reduction to 126.46 dB. The mass of the sandwich structure after the GA and MMA optimizations has increased by 4.9% and 6.4% respectively, while the hybrid optimization gave a mass enhancement of 5.7%. The hybrid GA-MMA method for the loading case 'a' results in a configuration with the minimum objective function and minimum mass increase.

Table 7: The optimization variables, loading case ‘a’

Configuration Set	θ_1	θ_2	θ_3	θ_4	θ_5	θ_6	θ_7	θ_8	θ_9	RMSL (dB)	Mass (Kg)
Base Line Configuration	-30	-30	-30	-30	-30	-30	-30	-30	-30	127.09	5.635
GA Optimized Configuration	-48.72	-49.31	46.33	-48.76	-48.42	-49.48	2.88	-46.64	-48.74	126.50	5.911
MMA Optimized Configuration	-50	-50	-30.68	-50	-50	-50	3.24	-50	-50	126.47	5.994
Hybrid MMA-GA Optimized Configuration	-50	-50	48.95	-50	-50	-50	0.01	-50	-50	126.46	5.956

Table 8: The optimization variables, loading case ‘b’

Configuration Set	θ_1	θ_2	θ_3	θ_4	θ_5	θ_6	θ_7	θ_8	θ_9	RMSL (dB)	Mass (Kg)
Base Line Configuration	-30	-30	-30	-30	-30	-30	-30	-30	-30	143.59	5.635
GA Optimized Configuration	-49.3	-41.95	-49.72	-48.5	-48.64	-49.04	-47.93	-43.69	-49.14	143.07	6.060
MMA Optimized Configuration	-50	-40.39	-50	-50	-50	-50	-50	-40.39	-50	143.04	6.077
Hybrid MMA-GA Optimized Configuration	-50	-40.39	-50	-50	-50	-50	-50	-40.39	-50	143.04	6.077

It is clear from Table 8 that for loading case ‘b’ the root mean square of the sound power level is reduced to 143.07 dB using GA optimization method. Applying both MMA and hybrid optimizations the RMSL is reduced to 142.04 dB. For the loading case ‘b’ all the optimized configurations have higher weight than the base line configuration. The optimized GA configuration results in 7.5% mass increase, while the MMA and hybrid optimized configurations show a 7.8% increase in mass. In the MMA optimized configuration, all the angles in the 9 regions are either -50^{o} or -40^{o}. The objective function for a sandwich structure with a non-gradient core with an internal angle of -10 and -50 is 144.12 dB and 143.07 dB, respectively. These results show that the use of a gradient topology in the sandwich structure core enables the structure slightly decrease the sound radiated power, at the same time giving a distribution of varying mechanical properties. Figure 33 and Figure 34 illustrate the core geometries for the different configurations of Table 7 and Table 8, respectively. For both loading cases the proposed core geometries of the GA optimized configuration and Hybrid configuration seems to be similar with slight change in cell angles in some regions.

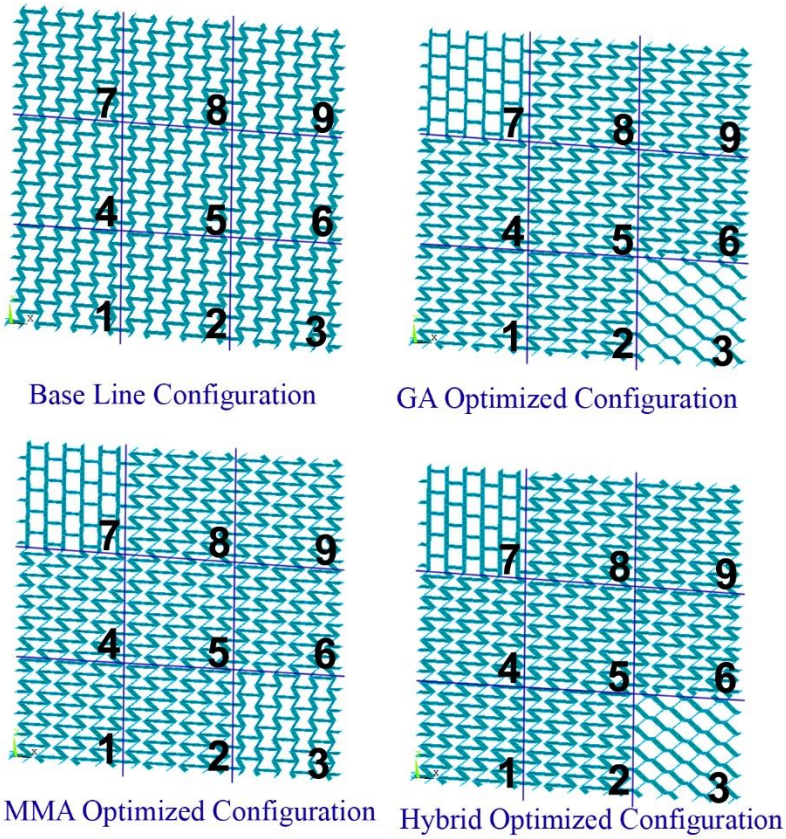

Figure 33: Core geometries of all configurations, loading case ‘a’

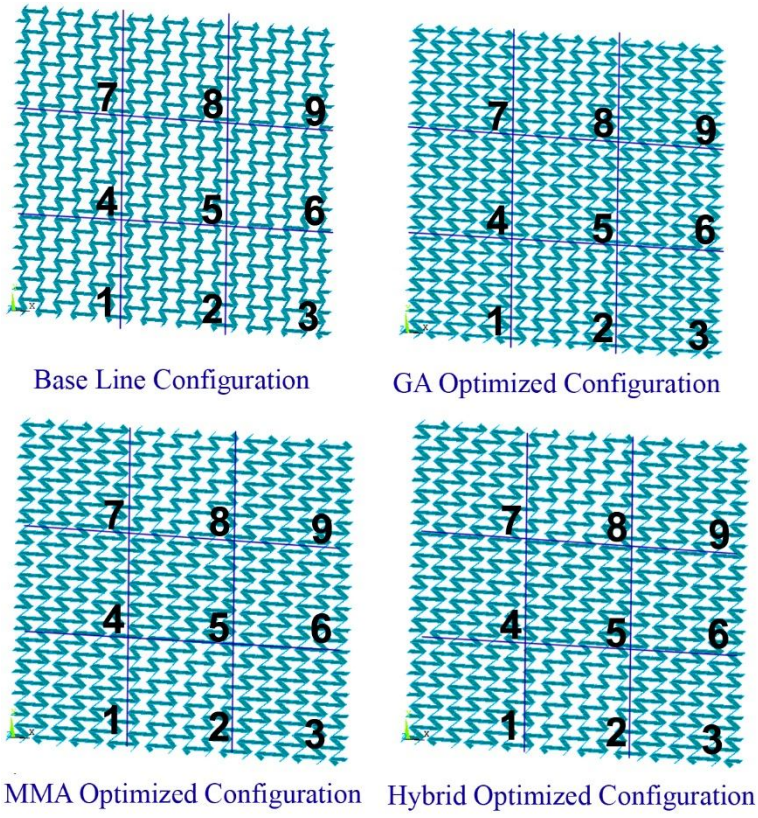

Figure 34: Core geometries of all configurations, loading case ‘b’

5.5.2 RSPL vs Frequency

Figure 35 shows the RSPL over the frequency range of 0-200 Hz for the four configuration sets under the loading case ‘a’. In these simulations, the thickness of the sandwich structure for all four cases is fixed in every part of the plate. For the loading case ‘a’ all optimum configurations show approximately similar RMSL-frequency curves. In the base line configuration, the peaks corresponding to all six natural frequencies within the considered bandwidth can be observed. On the contrary, in every optimum configuration, the peak corresponding to the 6^{th} natural frequency is missing within the same band. The peaks amplitudes are also reduced by 6 dB and 4 dB for the first and fourth natural frequency, respectively. It is also apparent that all the natural frequencies for the optimum configurations have shifted to lower values.

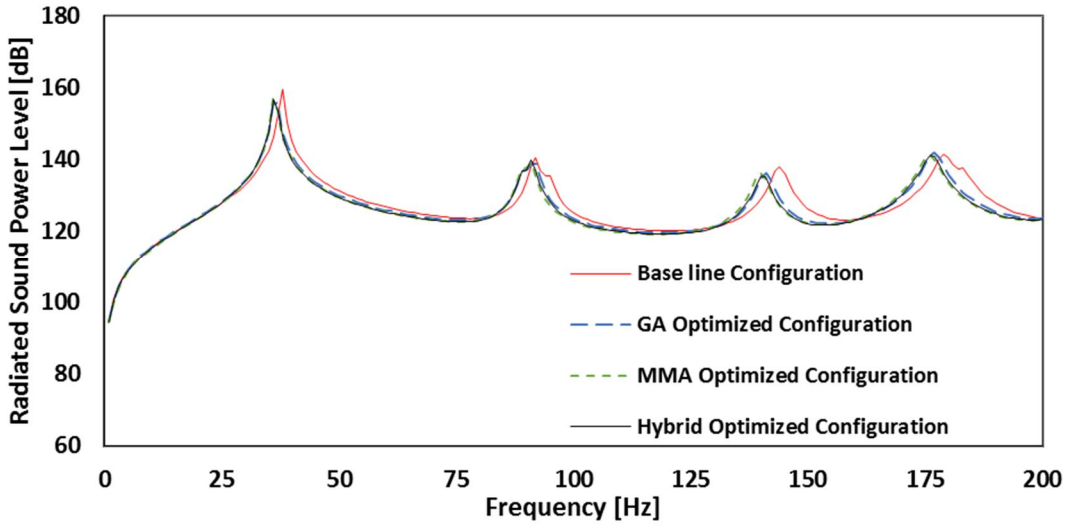

Figure 35: Effect of different optimization methods on sound power level reduction, loading case ‘a’

Figure 36 shows the RSPLs in the frequency domain for the four unique final optimized configurations subjected to loading case ‘b’, this time. It is worth mentioning that in this loading case the pressure is applied to the whole surface, and only modes 1, 5 and 6 are significantly excited. In this loading case, the change in the

first natural frequency for the optimum configurations is not significant. The 5th natural frequency is however decreased, while the 6th is out of the 0-200 Hz frequency range.

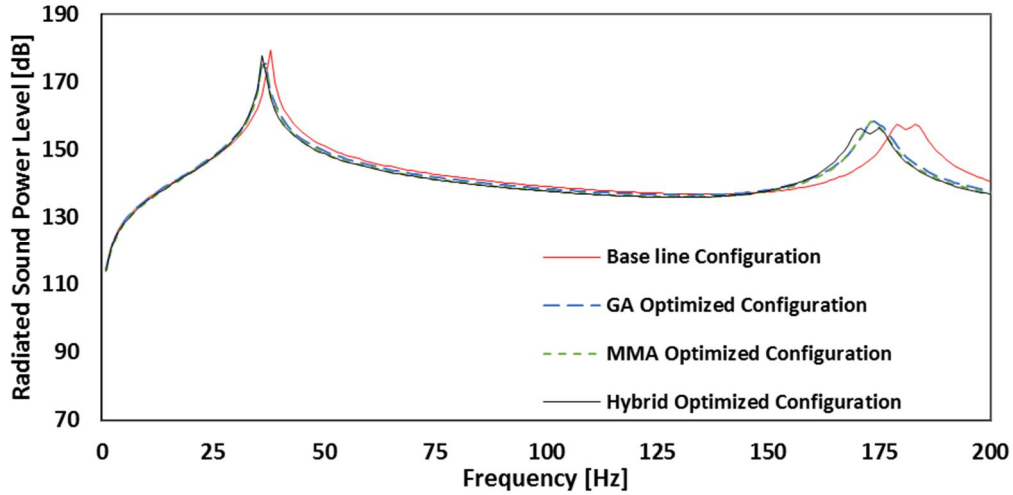

Figure 36: Effect of the different optimization methods on the sound power level reduction, loading case 'b'

5.5.3 Harmonic Analysis Results Verification

In chapter 3, the proposed homogenized model was validated comparing the result of the modal analysis for the homogenized model and the exact FE model. Here, the second model verification is done comparing the result of the harmonic analysis for the homogenized model and exact FE model. To verify the results corresponding to the loading case a, the frequency RSPL history related to the optimized Hybrid MMA-GA optimized configuration is shown in Figure 37 against the same configuration represented this time by a exact FE model. The RSPL represented by the homogenized model is a good approximation of the one provided by the exact FE one within the frequency range of 0-100 Hz. The exact FE model tends to provide a softening of the natural frequencies, but also a lower RMSL response. At higher frequencies the discrepancy between the results from the asymptotic homogenization model and the

exact FE one becomes larger; the homogenized model shows a lower modal density compared to the exact FE one.

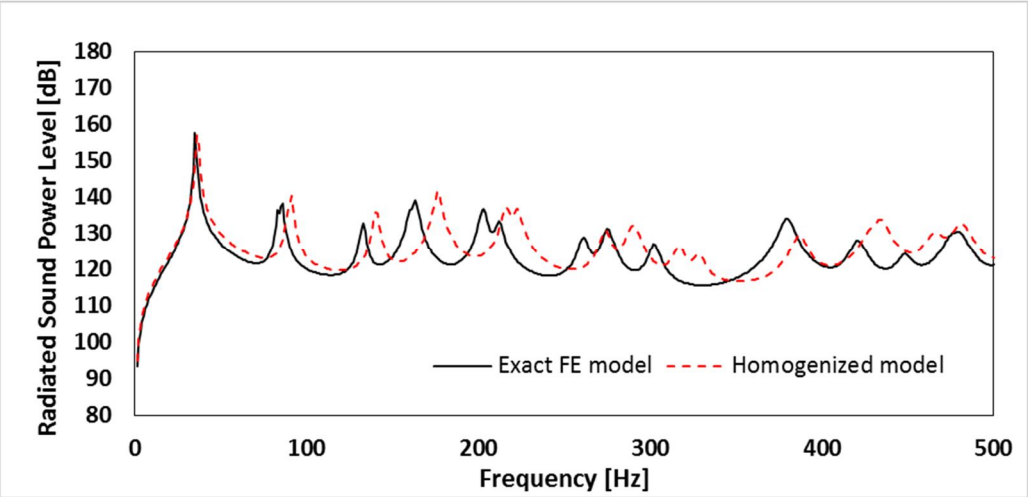

Figure 37: RSPL for the exact FE and the homogenized model, loading case ‘a’

5.5.4 RMSL Results Comparison

After result verification, in this section, the RMSL results of gradient sandwich structures is compared to the result of non-gradient sandwich structure. The loading condition for this comparison is considered to be the loading case ‘a’. Table 9 shows the RMSL and total mass for the five assorted configurations. The first configuration is a sandwich structure with a non-gradient conventional hexagonal honeycomb core with an internal angle of 30º. The second one is the base line configuration of this study which is related to a sandwich structure with a none-gradient auxetic core with internal an angle of -30º. The third configuration is the best configuration derived from Figure 23, i.e. a sandwich structure with a non-gradient auxetic core with internal an angle of -50º. The fourth configuration is a sandwich structure with 1-dimensional gradient core, similar to the one studied by Ranjbar et al. [45]. The fifth configuration is the Hybrid GA-MMA optimized configuration of this study (see Table 8) which is a sandwich structure with two-dimensional gradient core.

Table 9: Comparison of RMSL and mass for gradient and non-gradient topologies

Config. No.	Dimension [mm]	Core properties	Mass [kg]	RMSL[dB]
1	$996 \times 960 \times 20$	The core is a uniform conventional hexagonal topology with constant angle of 30º	5.221	127.77
2	$996 \times 960 \times 20$	The core is a uniform auxetic hexagonal topology with constant angle of -30º	5.635	127.09
3	$996 \times 960 \times 20$	The core is a uniform auxetic hexagonal topology with constant angle of -50º	6.143	126.51
4	$996 \times 960 \times 20$	The core is a 1-D gradient auxetic hexagonal with 3 different angles[45]	6.015	126.49
5	$996 \times 960 \times 20$	The core is a 2D gradient auxetic hexagonal with 9 different angles (the proposed configuration of this study)	5.956	126.46

The RMSL for the first configuration which is a sandwich structure with a conventional hexagonal honeycomb core is 127.77 dB while the RMSL for the second configuration, a sandwich structure with uniform auxetic gradient core with an internal angle of -30º, is 127.09 dB. This decrease of 0.7dB is considered to be a noticeable reduction in the root mean square level of radiated sound power level (RMSL). The RMSL for the third configuration which is a non-gradient sandwich structure with an internal core angle of -50º the analogous sound level is 126.51 dB. By using a gradient topology one obtains a decrease of the RMSL with a slight increase in mass compared to base line configuration. Compared to configuration No. 3, the 2D gradient configuration (configuration No. 4) shows, however, a slight reduction in RMSL, accompanied by 3% reduction of the total mass. This confirms that the gradient topology features a better performance compared to non-gradient one since the desired mechanical properties can be available in different regions. Moreover, because in the

2D gradient the change in topology is applied in two dimensions the RMSL is reduced to a lower value compared to a correspondent 1-D gradient topology. Different areas of the core have different transverse shear properties that affect the out-of-plane response at different resonant acoustic radiating modes.

5.5.5 Thickness Optimization of the Sandwich Structure

In this section, the effect of the change of sandwich structure's thickness, b, (see Figure 7) on the RMSL and the RSPL of the sandwich structure is demonstrated.

First, the effect of the change of the core thickness on the RMSL of the sandwich structure with a constant cell angle of -30^{o} has been evaluated. Figure 38 shows the RMSL results for both loading cases ‘a’ and ‘b’. The increase of the thickness creates a reduction of the RMSL for both loading cases. This reduction in RMSL generally happens since the increase in the core thickness leads to increased flexural properties of the sandwich structure. The thickness of 30 mm (that corresponds to the maximum of the thickness range considered) is considered to be an optimum thickness for both loading cases.

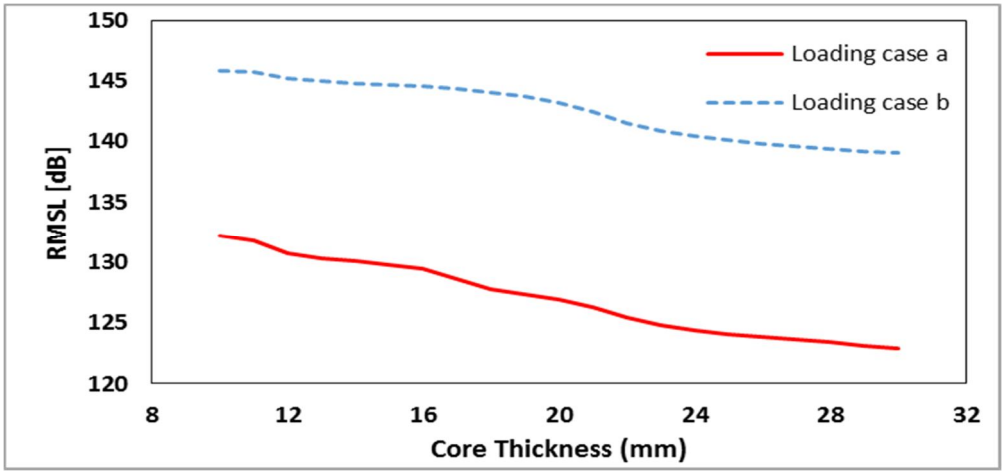

Figure 38: Variation of the RMSL with respect to the change of core thickness, constant internal cell angle of -30^{o} is considered for all cases

Next, the variation of the RSPL over the frequency range of 0-200 Hz for three different configurations have been compared to each other. The first configuration is the base line configuration of the study (see Table 7), the second configuration is a configuration with the original angles and optimum thickness, and the third configuration is a sandwich structure which has optimum angles (see Table 7) and optimum thickness. For the optimum thickness configurations, all natural frequencies are moved to higher values. The variation of the RSPL with respect to the frequency for these three configurations have been demonstrated in Figure 39. As it can be seen in the figure, for the optimum thickness and angles configuration only the first four natural frequencies remain within the 0-200 Hz range, and the 5th and 6th natural frequencies are now shifted to 226 Hz and 238 Hz, respectively.

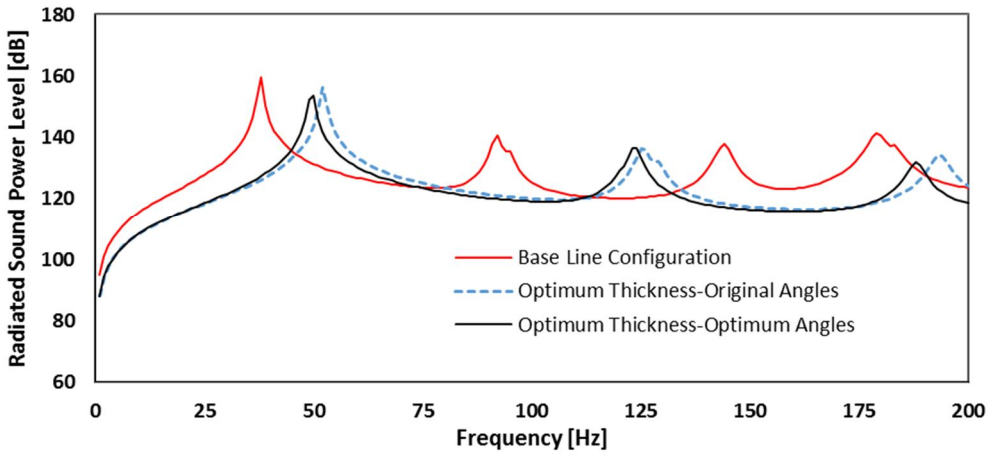

Figure 39: Sound power level reduction for the optimum thickness configurations, loading case 'a'

5.5.6 Normalized RSPL

The various optimized configurations bring a decrease of the RSML, but also marked changes of the mass of the panels. To account for the change of weight, a normalized acoustic sound power $(\bar{P})$ should be evaluated, calculated as the ratio between the

radiated sound power $P_{acoustic}$ and the power associated with the kinetic energy T of the structure [45]:

$$\bar{P} = P_{acoustics} / T \tag{30}$$

$$T = \frac{1}{2} m_t \omega^3 S \tag{31}$$

In Equation 31 the kinetic power is defined in term of the circular frequency of the harmonic excitation pressure loads, ω (in s^{-1}), the total mass of the sandwich structure, m_t (in kg), and the radiating area of sandwich structure S. The normalized frequency ω_n is also defined in Equation 32, where ω_1 is the first natural frequency of the base line configuration.

$$\omega_n = \frac{\omega}{\omega_1} \tag{32}$$

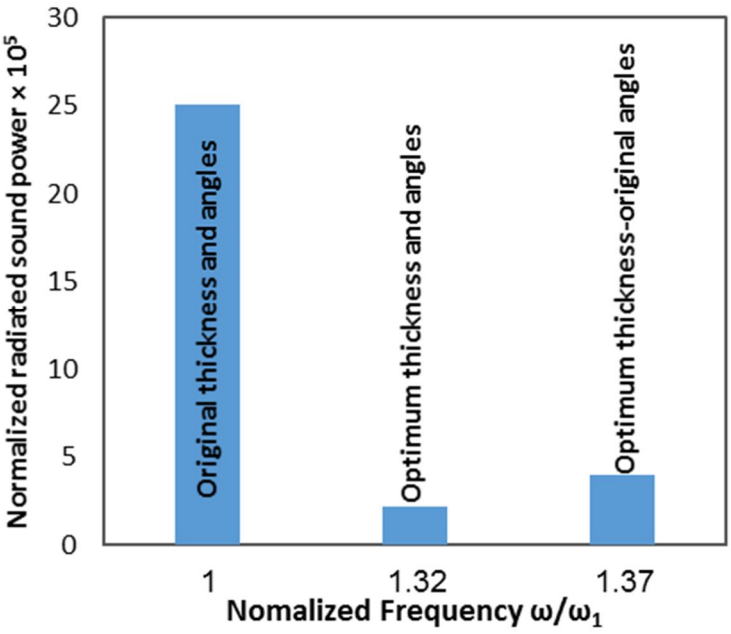

Figure 40: Normalized radiated sound pressures at non-dimensional frequencies, loading case 'a'

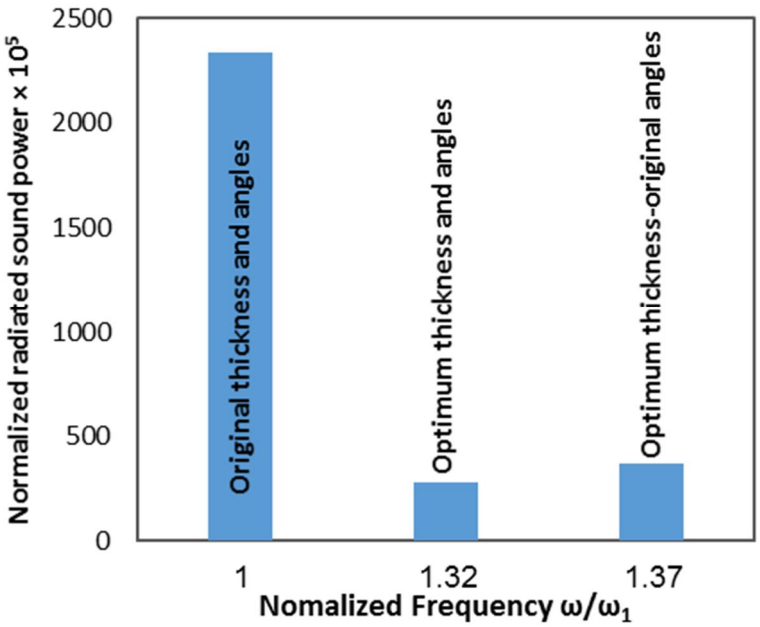

Figure 41: Normalized radiated sound pressures at non-dimensional frequencies, loading case 'b'

Figure 40 and Figure 41 show the reduction of the normalized radiated sound power with respect to the thickness and angle variation in the hexagonal honeycomb sandwich structure for loading cases 'a' and 'b', respectively. For the two loading cases, the optimum configurations feature a normalized fundamental frequency shifted to higher values by 32% and 37%. What is quite remarkable is the 91.1% reduction in the normalized radiated sound power for the configuration with optimum thickness and cell angles. For the original angles of -30^{o} and the optimum thickness of 30 mm, the normalized radiated sound power is also decreased by 84.2%. In the loading case 'b', the increase in normalized frequency for the original angles and optimum thickness configuration and the optimum thickness and cell angles configuration are 37% and 32%, respectively. The optimized configuration show also, in this case, a remarkable decrease of the normalized radiated sound power of 84.2% and 87.2%. The normalized sound power level is significantly higher in the loading case 'b' than loading case 'a' since in this loading case the same pressure is applied to a larger area.

5.6 Concluding Remarks

This study has shown that the variation of out-of-plane mechanical properties of auxetic hexagonal honeycombs in uniform and 2D gradient configurations lead to a reduction in the RSPL. The use of auxetic core increases, however, the total mass of the sandwich structure. To overcome this drawback, a gradient core can be used because of the capability of tailoring the mechanical properties. The radiated noise level of the structure is also significantly dependent upon the location of the excitations. The use of gradient core geometries can be instrumental to cover the excitations areas.

A simple non-gradient sandwich structure radiates less sound compared to a simple plate with the same mass, and this is due to the increased flexural properties of the sandwich structure. The RMSL for a sandwich structure with a non-gradient core changes between 126.51 dB and 127.83 dB. The use of a gradient topology leads to a decrease of the RMSL, with a slight increase in mass compared to the base line non-gradient configuration with an internal angle of -30^{o}. Moreover, this optimized gradient sandwich structure shows a slight reduction in RMSL accompanied by a 3% reduction in mass compared to a non-gradient sandwich structure with an internal angle of -50^{o}. This confirms that the gradient topology has an enhanced performance compared to the non-gradient one, as optimized mechanical properties can be available in different regions. The 2D gradient core appears to offer a reduced RMSL compared to the 1-D gradient topology. The reduction becomes however remarkable when the normalized RSPLs and frequencies are considered. In those cases, the 2D gradient with both thickness and optimized cell angles provide a very significant reduction (91%) of the normalized power of the radiated sound, compared to the base line configuration.

In this work the Genetic algorithm, the method of moving asymptotes and the hybrid GA-MMA optimizations methods have been used to optimize the root mean square of the sound power level. The computation time related to the MMA calculations was 93% lower than the one needed for the GA optimization. In all loading cases, it has been noticed that the configuration proposed by the hybrid GA-MMA optimization method performs better in reducing the RSPL. This reduction in RMSL is accompanied by an increase in the total mass of the structure by 5.7 % and 7.8% for the loading cases ‘a’ and ‘b’, respectively. This configuration behaves significantly better than the base line one, both in low and higher frequency ranges. For the two loading cases, the GA optimized configuration has the smallest mass increment compared to the base line configurations, while the objective function is significantly reduced. This feature could be considered for structures applications for which weight reductions are paramount.

Chapter 6

OPTIMIZATION OF THE 2D GRADIENT ANTI-TETRACHIRAL SANDWICH STRUCTURE

6.1 Introduction

This chapter deals with vibroacoustic behavior of sandwich structure with anti-tetrachiral core. Chiral lattices have attracted the attention of researchers as their unique topology brings outstanding features such as high strength, lightweight and excellent design flexibility [53]. Anti-tetrachiral lattices have been used previously as a core in sandwich structure to optimize the radiated sound from a sandwich structure [45]. In the study mentioned before the total mass of a sandwich structure was not considered as a constraint. However, in this study, a mass constrained optimization will be accomplished. Section 6.2 introduces the gradient topology in anti-tetrachiral cores. Section 6.3 and 6.4 explains the RMSL optimization result of the 2D gradient anti-tetrachiral sandwich structure and finally, in section 6.5, the normalized RSPL of these sandwich structure has been evaluated.

6.2 Gradient Topology

As it has been investigated before, using gradient topology in a sandwich structures core will lead to have desired mechanical properties in different areas of the core [45], [74]. Here, for the sandwich structure with anti-tetrachiral core using gradient geometry will lead to better vibroacoustical behavior. The same concept has been adopted in chapter 5 for the auxetic hexagonal honey comb cores.

6.2.1 Variation of RMSL with Respect to Change of Cell Radius

Before introducing gradient topology for the core of the sandwich structure, the change of RMSL with respect to the change of cell radius should be investigated. Figure 42 shows this variation. The homogenized modeling introduced in Chapter 3 is used to analyze the auxetic anti-tetrachiral sandwich structure. The geometrical parameters of the core have been given in Table 4 and the anti-tetrachiral core is covered with two 960×960×2 mm skins plates. Both core and skins are made of ABS plastic with elastic properties listed in [44].

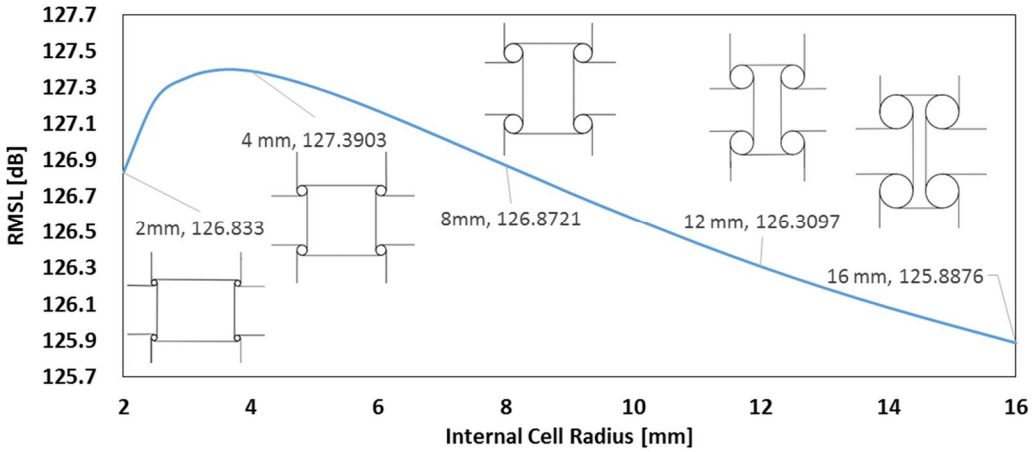

Figure 42: The variation of RMSL with respect to change in internal cell radius

The RMSL in the sandwich structures with higher core internal cell radii is generally lower than the RMSL in sandwich structures with lower internal cell radii. The Maximum RMSL happens at cell radius of 3.5 mm while it can be noted that the sandwich structure with a core internal cell radius of 16 mm shows the minimum RMSL.

In the next section, a gradient topology for the anti-tetrachiral core of the sandwich structure will be proposed and the effect of this topology on the vibroacoustic behavior of the sandwich structures will be investigated.

6.2.2 Defining Gradient Geometry

The core geometry of the sandwich structure in section 6.2.1 was a uniform core geometry. In another word, the core cellular structure was made of cells having the same geometry in any part of the structure. It is, however, possible to produce this cellular structure with a gradient configuration. The configuration in this gradient topology is made of a continuous distribution of unit cells with compatible geometry, but having a single variable parameter like the internal cell radius. In gradient configuration, using a gradient cellular structure will lead to a varying distribution of stiffness and deformation. Therefore, different mechanical properties can be achieved in different areas of the structure. Having desired mechanical properties in the various regions of the core will lead to having better vibroacoustical behavior [45].

Figure 43 shows an example of a 2D gradient anti-tetrachiral core configuration. As it can be seen in this figure the core geometries in different regions are different. The 2D gradient core consists of nine different regions with nine different internal radii, *r*.

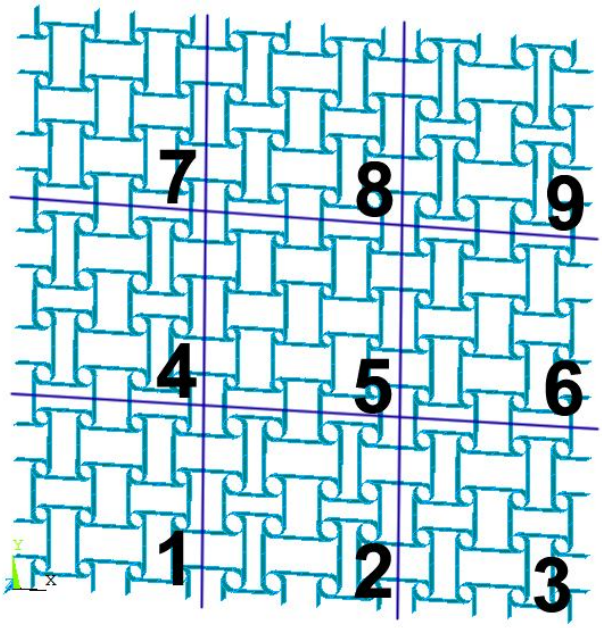

Figure 43: Gradient anti-tetrachiral core with nine different regions

Figure 44 shows a gradient geometry for an anti-tetrachiral unit cell. To generate the 2D gradient core configuration, the unit cells have been assembled next to each other. The ligament length, L shown in the figure is fixed. Therefore, these unit cells can be simply assembled next to each other in x and y-direction to form the 2D gradient core. The geometry and mechanical properties of the unit cells will change with a change in cell radius, r, while the length L_1 is fixed. The formula proposed in Chapter 3 can be used to determine the mechanical properties in each region. The geometrical parameters of the base line anti-terachiral unit cell have been shown in Table 4.

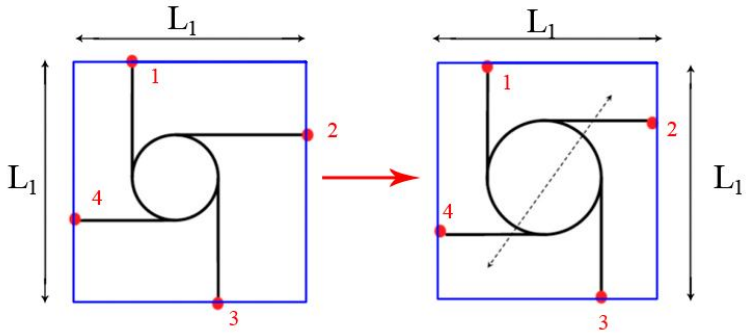

Figure 44: Gradient geometry for a unit cell with changing radii and fixed ligament length, L_1

The distribution of the homogenized anti-tetrachiral unit cells for the 2D gradient topology is same as the distribution of the hexagonal honeycomb core and it has been shown in Figure 26. The nine different regions with nine different cell radii (r_1, r_2, r_3, r_4, r_5, r_6, r_7, r_8, r_9) are assembled next to each other to form the whole sandwich structure. Each region is shown with a distinct color. The main objective of the optimization problem is to minimize the RMSL by modifying the geometry of the model in each of these 9 regions.

In the following section, the minimization of the RSPL for the sandwich structures with 2D gradient core will be presented.

6.3 RMSL Optimization of the 2D Gradient Sandwich Structure

The minimization process of RSPL over the frequency range of 0 to 200 Hz is discussed in this section. The objective function for the optimization process is the root mean square level of radiated sound power level (RMSL) of sandwich structure. The design variables of this optimization problem in this section are the internal cell radii in the different regions as well as the core thickness, b, the ligament thickness, t_l and the skin thickness, t_s. The total number of design variables is 12 as there are 9 different cell radii in different regions and there are 3 different thicknesses. The geometrical parameters for base line configuration of the sandwich structure are given in Table 10.

Table 10: Geometrical parameters of the base line anti-tetrachiral core

r (mm)	L_x(mm)	L_y(mm)	t_l (mm)	b (mm)	t_s (mm)
8	24	24	1	12	2

The sandwich structure which is considered to be the base line configuration of this study consists of a uniform core with a constant cell radius of 8 mm. The total mass, m_t, of this sandwich structure is 5.341 kg. The optimization process in this chapter is a mass constrained optimization. The maximum increase in the total mass of the optimized design of the sandwich structure is considered to be 10% increase in total mass of the base line configuration, m_b.

Therefore, the general optimization problem is, then defined as:

Minimize RMSL$\left(r_1, r_2, r_3, r_4, r_5, r_6, r_7, r_8, r_9, t_l, t_s, b\right)$

S. t.

$$3mm \le \left(r_1, r_2, r_3, r_4, r_5, r_6, r_7, r_8, r_9\right) \le 16mm \tag{33}$$

$$1mm \le t_l, t_s \le 2mm$$

$$0.9\, m_b \le m_t \le 1.1\, m_b$$

To do the optimization process two different optimization methods have been considered. The Genetic Algorithm optimization method (GA) and the Method of Moving Asymptotes (MMA) [59], [66].

6.3.1 GA Optimization

Genetic algorithm has been widely used in topology optimization problems. In this section, GA optimization technique is used to minimize the radiated sound from a sandwich structure. The design variables have been defined in the previous section. Here, unlike the optimization process for hexagonal honeycomb sandwich structure in Chapter 5 the core thickness, ligament thickness and the skin thickness are not fixed and considered to be design variables of the optimization problem. The procedure to apply the Genetic algorithm optimization method is same as the one defined in Chapter 5 and the flow chart this procedure has been demonstrated in Figure 27.

As mentioned before, the optimization problem is described by twelve design variables. Therefore, selecting a proper population size is a challenge. In order to do that a sensitivity analysis on the order of population size has been performed and the initial population size of 50 is considered. For a better scoping of the feasible design envelope of this optimization problem, the first generation of the genetic algorithm has been created by using a Latin hypercube sampling (LHS) method. Figure 28 shows the plot matrix of the LHS design and the related objective function.

As it is shown in the figure the design variables created by LHS method are evenly distributed within their defined range. The thirteenth row and column show the RMSL which is the objective function of this optimization problem while the fourteenth row and column illustrate the total mass of the sandwich structure. It can be observed that the reduction in the RMSL generally is accompanied by an increase in the total mass. Moreover, an increase in ligament thickness, t_l, leads to reducing the RMSL. Also, the core thickness, b, is an effective factor on RMSL and the increase in core thickness causes RMSL to decrease. Next, it should be mentioned that an increase in any of the thicknesses leads to increase in the total mass of the sandwich structure as the density of the sandwich structure increases.

After having the initial population created by LHS design method, the objective function is then minimized over 100 generations. The crossover probability is 0.8 and the mutation rate is 0.2. Figure 46 shows the variation of the best and the average of the objective function at each generation for the loading case ‘a’. The convergence is observed after about 80 generations. Each function evaluation takes about 4.5 CPU seconds on a 2.6 GHz Intel® Core™ i5 processor with 4 GB of RAM operating on a Windows 7 system. The total computation time using the GA method was about 6 hrs. and 15 minutes.

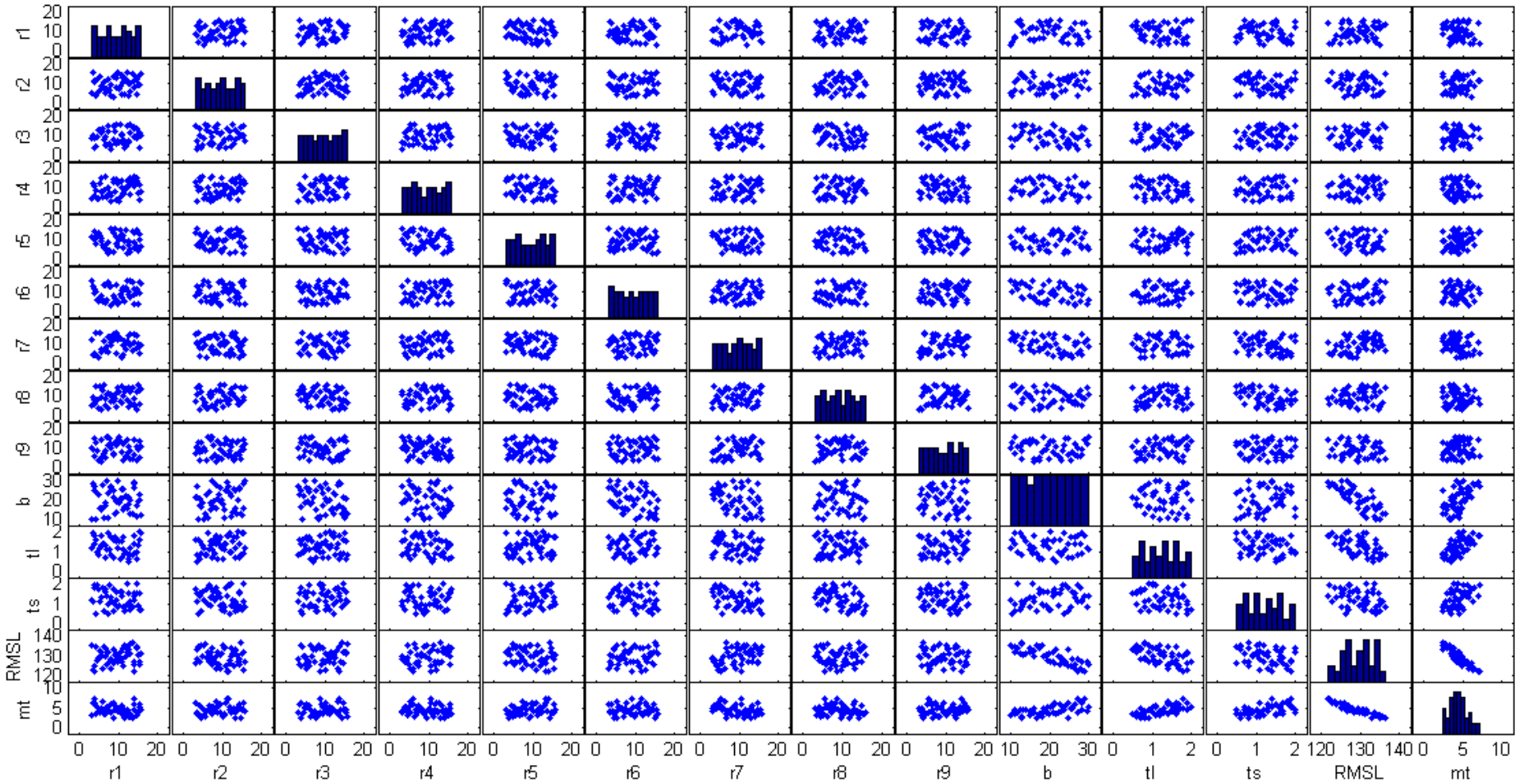

Figure 45: Plot matrix of Latin Hypercube Sampling for the GA initial population, The RMSL is calculated for load case ‘a’

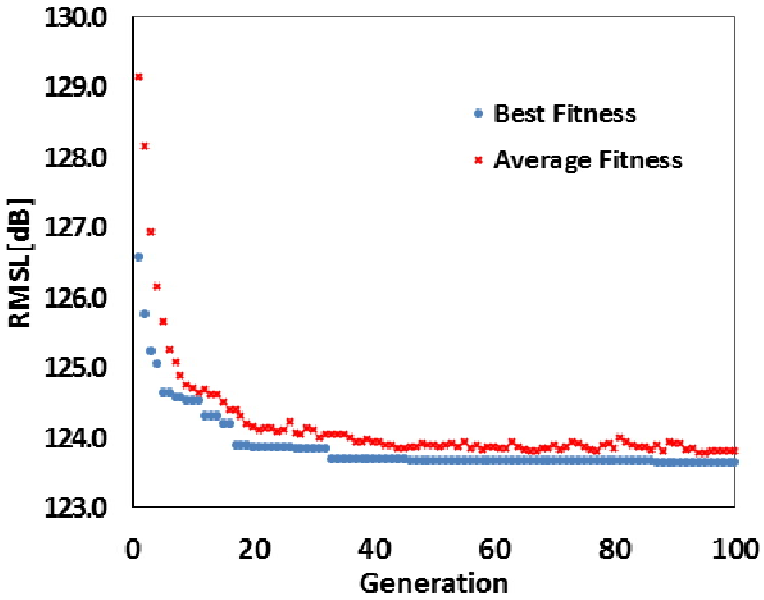

Figure 46: Variation RMSL per generation during the GA optimization for loading cases 'a'

6.3.2 MMA Optimization

The other method evaluated in this study for optimization purposes is the Method of Moving Asymptotes (MMA) [59], [66]. For the first iteration, an initial guess of the design variables, θ_k, is required. The initial guess of the design variables in this research is considered to be:

$$\theta_k = \{8mm, 8mm, 8mm, 8mm, 8mm, 8mm, 8mm, 8mm, 8mm, 1mm, 2mm, 20mm\}$$

The change of the objective function per iteration is demonstrated in Figure 31. It can be observed that the convergence occurs after 8 iterations in this case. It should, however, be mentioned that, as the MMA is a gradient-based method, each iteration includes in this case 18 function evaluations (sub-iterations). Nevertheless, the MMA features a decrease in computation time to 27 minutes.

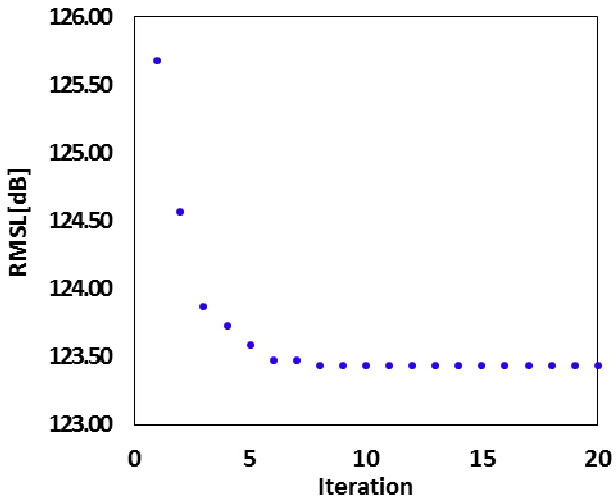

Figure 47: Variation of RMSL per iteration in MMA optimization method, loading cases ‘a’

6.4 Optimization Results

In this section, the base line configuration and all optimal configurations of the anti-tetrachiral sandwich structure have been compared. The base line configuration is a sandwich structure with total dimensions of $960\times960\times20$ mm. The core of this sandwich structure consists of 12×12 anti-tetrachiral unit cells with an internal cell radius of $r=8mm$. The core is covered with two 960×960×2 mm skins plates. Both core and skins are made of ABS plastic with elastic properties listed in [44]. The geometrical parameters of the model are given in Table 10. All the optimized configurations have the same total dimensions, material properties as the base line configuration. The only difference is that they have different internal cell radii, {r_1, r_2, r_3, r_4, r_5, r_6, r_7, r_8, r_9}, in different regions of the core. Moreover, they can have varied ligament thickness, t_l, skin thickness, t_s and core thickness, b.

6.4.1 RMSL Optimization ResultsTable 11 shows the geometry, optimization variables and total mass of the sandwich structure for the base line and optimal configurations. The GA reduced the root mean square of sound power level to 123.66 dB, while the MMA reduced the objective function to 126.29 dB. The mass of the

sandwich structure after the GA and MMA optimizations has increased by 10% which was the upper bound defined in the mass constrained optimization problem. In the MMA optimized configuration, the cell radii in regions 2, 5 and 6 are 16 mm which is the upper bound for the radii. It can also be noted that the core thickness, b, is at its maximum defined value which is 25mm. The skin thickness, t_s, is 2 mm and the ligament thickness, t_l, is 1mm. These results show that the use of a gradient topology in the sandwich structure core as well as enhanced core thickness enables the structure to decrease the sound radiated power, at the same time giving a distribution of varying mechanical properties. Figure 48 demonstrates the core geometry of the base line configuration and MMA optimized configuration.

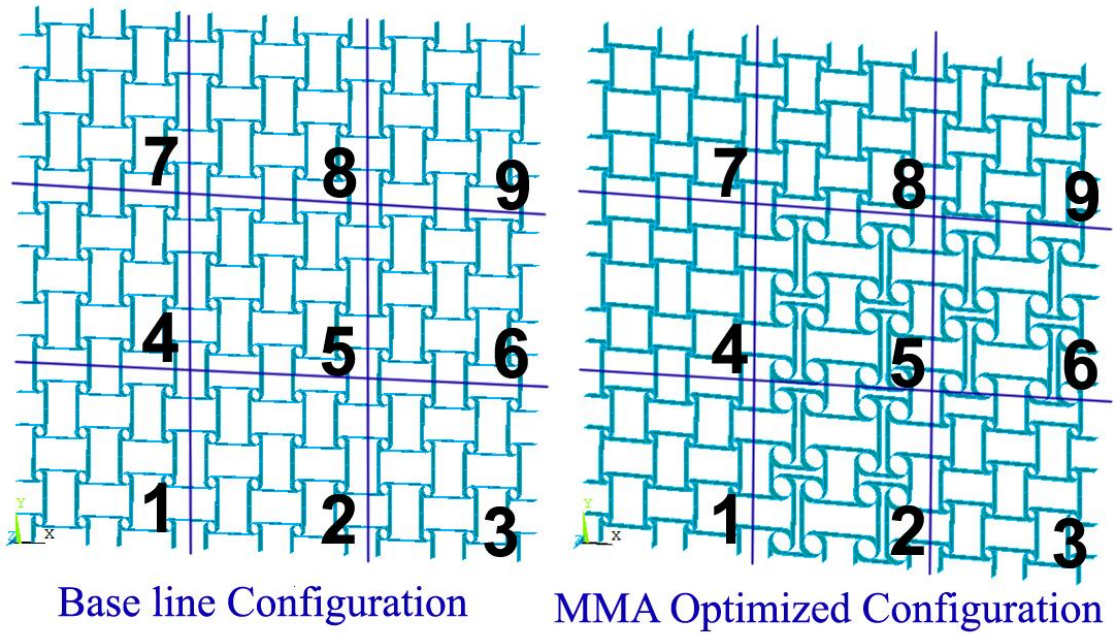

Figure 48: Core geometry of the base line configuration and the optimized configurations

Table 11: The optimization variables for the anti-tetrachiral sandwich structure

Configuration Set	r_1(mm)	r_2(mm)	r_3(mm)	r_4(mm)	r_5(mm)	r_6(mm)	r_7(mm)	r_8(mm)	r_9(mm)	t_l(mm)	t_s(mm)	b(mm)	RMSL (dB)	Mass (Kg)
Base line Configuration	8	8	8	8	8	8	8	8	8	1	2	20	126.87	5.341
GA Optimized Configuration	5.7	10.6	14.4	9.3	15.4	16	12.6	14.1	14.6	0.91	1.96	25	123.66	5.875
MMA Optimized Configuration	5.84	16	7.96	3	16	16	3	7.85	10.3	1	2	25	123.29	5.875

6.4.2 RSPL vs Frequency

Figure 49 shows the RSPL over the frequency range of 0-200 Hz for the three configuration sets under the loading case ‘a’. Both optimum configurations show approximately similar RSPL-frequency curves. In the base line configuration, the peaks corresponding to all six natural frequencies within the considered bandwidth can be observed. It should be noted that as the anti-tetrachiral core is a transversely isotropic material, i.e. the core material properties in x and y-direction are same, the 2^{nd} and 3^{rd} modes and also 5^{th} and 6^{th} modes happen at the same natural frequency. This is the reason that in this figure, four peaks can be observed instead of six peaks. For the optimum configurations, the peak corresponding to the 5^{th} and 6^{th} natural frequency is missing within the same band. The peaks amplitudes are also reduced by 8 dB, 6 dB and 4 dB for the first, second and the third peaks, respectively. It is also apparent that all the natural frequencies for the optimum configurations have shifted to lower values.

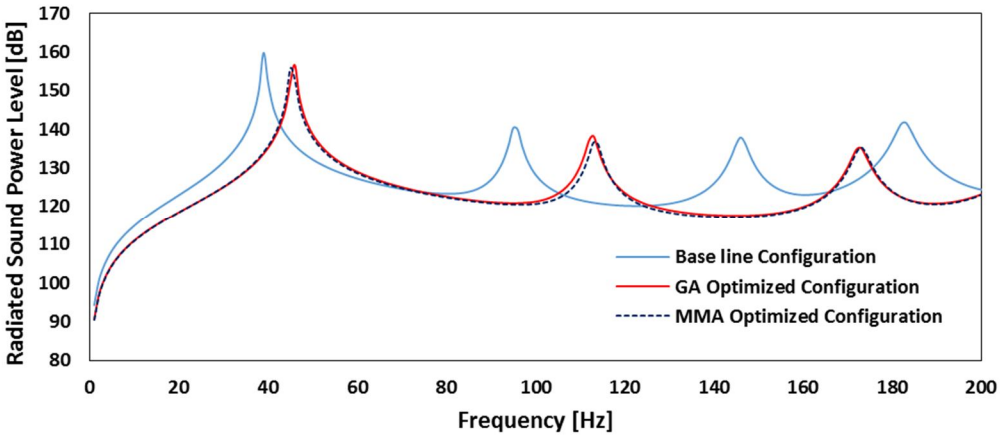

Figure 49: RSPL vs frequency, different anti-tetrachiral configurations

6.4.3 Harmonic Analysis Results Verification

In chapter 3, the proposed homogenized model was validated comparing the result of the modal analysis for the homogenized model and the exact FE model for the anti-

tetrachiral sandwich structure. Here, the second model verification is done comparing the result of the harmonic analysis for the homogenized model and exact FE model. To verify the results corresponding to the loading case a, the frequency RSPL history related to the MMA optimized configuration is shown in Figure 50 against the same configuration represented this time by an exact FE model. The RSPL represented by the homogenized model is a good approximation of the one provided by the exact FE one within the frequency range of 0-200 Hz. The homogenized model tends to provide the same curve of the exact FE model with a small shift of the peaks to the higher natural frequencies. At higher frequencies the discrepancy between the results from the asymptotic homogenization model and the exact FE one becomes larger; the homogenized model shows a lower modal density compared to the exact FE one.

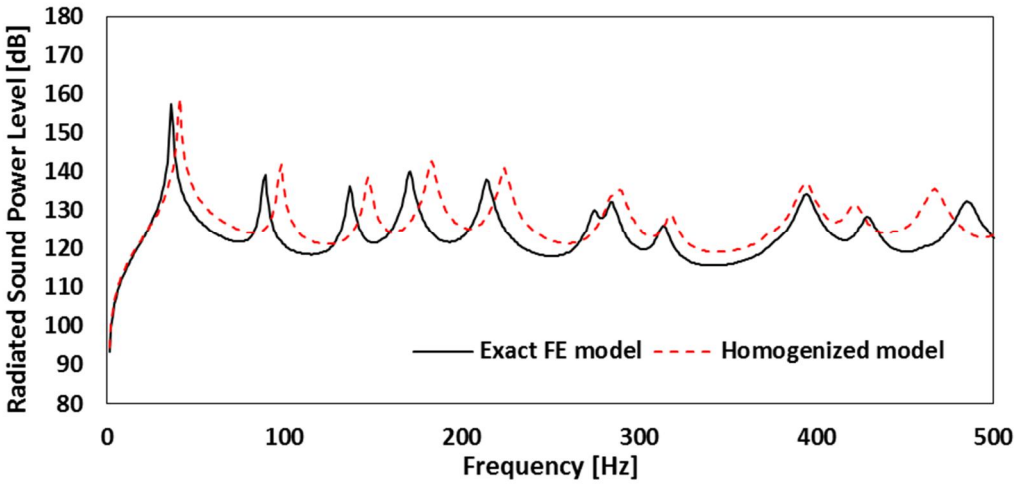

Figure 50: RSPL for the exact FE and the homogenized model, loading case ‘a’

6.4.5 Normalized RSPL

Figure 51 shows the reduction of the normalized radiated sound power with respect to the thickness and node radius variation in the anti-tetrachiral sandwich structure for loading cases ‘a’. The optimum configuration feature a normalized fundamental frequency shifted to higher value by 15%. What is quite remarkable is the 78.2%

reduction in the normalized radiated sound power for the configuration with optimum thickness and cell angles.

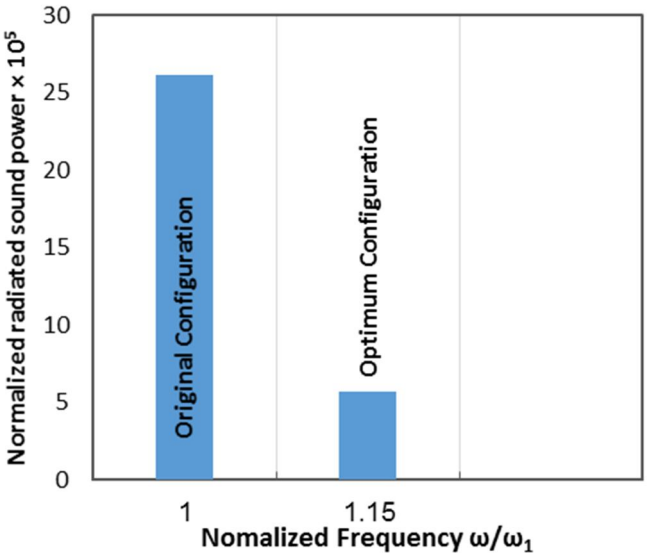

Figure 51: Normalized radiated sound pressures at non-dimensional frequencies, loading case 'a'

6.5 Concluding Remarks

This study has shown that the variation of out-of-plane mechanical properties of anti-tetrachiral sandwich structures in uniform and 2D gradient configurations lead to a reduction in the RSPL. The use of increased ligament thickness, skin thickness and core thickness will lead to a reduction in the RSPL of the sandwich structure, however, it will increase the total mass of the sandwich structure. To overcome this drawback, a gradient core can be used because of the capability of tailoring the mechanical properties. The radiated noise level of the structure is also significantly dependent upon the location of the excitations. The use of gradient core geometries can be instrumental to cover the excitations areas.

The RMSL for a sandwich structure with a non-gradient core changes between 125.9 dB and 127.4 dB. The use of a gradient topology, as well as increased thicknesses, lead to a decrease of the RMSL, with a defined increase in the total mass compared to the base line non-gradient configuration with an internal cell radius of 8mm. This confirms that the gradient topology has an enhanced performance compared to the non-gradient one, as optimized mechanical properties can be available in different regions. The reduction becomes however remarkable when the normalized RSPLs and frequencies are considered. In those cases, the 2D gradient with both thickness and optimized cell angles provide a very significant reduction (91%) of the normalized power of the radiated sound, compared to the base line configuration.

In this work, the Genetic algorithm and the method of moving asymptotes optimizations have been used to optimize the root mean square of the sound power level. The computation time related to the MMA calculations was 93% lower than the one needed for the GA optimization. The RMSL is reduced by 3.21 dB using GA optimization, while the MMA method reduces the RMSL by 3.58 dB. This reduction in RMSL is accompanied by an increase in the total mass of the structure by 10 % for both optimized configurations. The MMA optimized configuration behaves significantly better than the base line one, both in low and higher frequency ranges. The result of this study can be considered for structures applications in which the total mass of the structure plays an important role in the optimization process.

Chapter 7

CONCLUSION

In this study a 2D gradient topology for auxetic sandwich structure was developed and the homogenization approach was applied to determine the RMSL of this 2D gradient sandwich structure. Moreover, an optimization scheme was developed by integrating ANSYS with MATLAB to optimize the RMSL for the 2D gradient topology and finally, the RMSL was optimized by applying gradient base optimization method, Method of Moving Asymptotes and direct search method, Genetic Algorithm optimization. This procedure was applied for two different class of sandwich structure's core geometries. Case 1, Auxetic hexagonal honeycombs and case 2, Anti-tetrachiral lattices.

The result of this study has shown that the variation of out-of-plane mechanical properties of auxetic sandwich structures in uniform and 2D gradient configurations lead to a reduction in the RMSL. The use of auxetic core increases, however, the total mass of the sandwich structure. To overcome this drawback, a gradient core can be used because of the capability of tailoring the mechanical properties. The radiated noise level of the structure is also significantly dependent upon the location of the excitations. The use of gradient core geometries can be instrumental to cover the excitations areas.

In case 1, it was demonstrated that a simple non-gradient sandwich structure radiates less sound compared to a simple plate with the same mass, and this is due to the increased flexural properties of the sandwich structure. The RMSL for a sandwich structure with a non-gradient core changes between 126.51 dB and 127.83 dB. The use of a gradient topology leads to a decrease of the RMSL, with a slight increase in mass compared to the base line non-gradient configuration with an internal angle of -30^{o}. Moreover, this optimized gradient sandwich structure shows a slight reduction in RMSL accompanied by a 3% reduction in mass compared to a non-gradient sandwich structure with an internal angle of -50^{o}. This confirms that the gradient topology has an enhanced performance compared to the non-gradient one, as optimized mechanical properties can be available in different regions. The 2D gradient core appears to offer a reduced RMSL compared to the 1-D gradient topology. The reduction becomes however remarkable when the normalized RSPLs and frequencies are considered. In those cases, the 2D gradient with both thickness and optimized cell angles provide a very significant reduction (91%) of the normalized power of the radiated sound, compared to the base line configuration.

Then, the Genetic algorithm, the method of moving asymptotes and the hybrid GA-MMA optimizations methods have been used to optimize the root mean square of the sound power level. The computation time related to the MMA calculations was 93% lower than the one needed for the GA optimization. In all loading cases, it has been noticed that the configuration proposed by the hybrid GA-MMA optimization method performs better in reducing the RSPL. This reduction in RMSL is accompanied by an increase in the total mass of the structure by 5.7 % and 7.8% for the loading cases ‘a’ and ‘b’, respectively. This configuration behaves significantly better than the base line one, both in low and higher frequency ranges. For the two loading cases, the GA

optimized configuration has the smallest mass increment compared to the base line configurations, while the objective function is significantly reduced. This feature could be considered for structures applications for which weight reductions are paramount.

In case 2 it was shown that the use of increased ligament thickness, skin thickness and core thickness will lead to a reduction in the RSPL of the sandwich structure, however, it will increase the total mass of the sandwich structure. To overcome this drawback, a gradient core can be used because of the capability of tailoring the mechanical properties.

The RMSL for a sandwich structure with a non-gradient anti-tetrachiral core changes between 125.9 dB and 127.4 dB. The use of a gradient topology, as well as increased thicknesses, lead to a decrease of the RMSL, with a defined increase in the total mass compared to the base line non-gradient configuration with an internal cell radius of 8mm. This confirms that the gradient topology has an enhanced performance compared to the non-gradient one, as optimized mechanical properties can be available in different regions. The reduction becomes however remarkable when the normalized RSPLs and frequencies are considered. In those cases, the 2D gradient with both thickness and optimized cell node radii provide a very significant reduction (78%) of the normalized power of the radiated sound, compared to the base line configuration.

Moreover, genetic algorithm and the method of moving asymptotes optimizations have been used to optimize the root mean square of the sound power level. The computation time related to the MMA calculations was 93% lower than the one needed for the GA optimization. The RMSL is reduced by 3.21 dB using GA optimization, while the MMA method reduces the RMSL by 3.58 dB. This reduction in RMSL is accompanied

by an increase in the total mass of the structure by 10 % for both optimized configurations. The MMA optimized configuration behaves significantly better than the base line one, both in low and higher frequency ranges. The result of this study can be considered for structures applications in which the total mass of the structure plays an important role in the optimization process.

7.1 Highlights

- In the current literature, the gradient topology in the core geometry of the sandwich structure has always considered to be 1-D, i.e. the change in geometrical parameters were either in x or y-direction. In the current study, however, a novel 2D gradient toplogy in introduced in which the change in internal cell angle in the hexagonal honeycombs and the change in internal cell radii for the anti-tetrachiral lattices is in both x and y-directions.
- In the previous studies effect of change of a single geometrical parameter on the RSPL had been investigated, while in this research, effect of all of the core geometrical parameters on the RSPL was investigated.
- The optimization method which have been used to minimize the RSPL were to way simple. However in the present research, two powerful optimization methods have been implemented in order to obtain better results.
- In case 2, which was the RMSL optimization of anti-tetrachiral sandwich structure, the design variables include almost all geometrical parameters of the sandwich structure were considered as design variables which lead to have better options in tailoring mechanical properties of the structure. Moreover, the total mass of the sandwich structure were considered to be a design constraint for the optimization problem.

7.2 Future Works

- Further improvement on the RMSL can be achieved conducting the optimization on the exact FE model. In order to do that high computation efficiency is required.
- Several types of auxetic cores are available in the literature. Same RMSL minimization approach can be carried out for other types of core geometries.
- RMSL minimization approach can be used in different plate geometries such as circular sandwich structures.

REFERENCES

[1] M. Ranjbar, "A Comparative Study on Optimization in Structural Acoustics," *Technische Universität Dresden*, Germany, 2011.

[2] Y. Zhang, H. Wu, W. Jiang, and N. Kessissoglou, "Acoustic topology optimization of sound power using mapped acoustic radiation modes," *Wave Motion*, vol. 70, pp. 90–100, 2017.

[3] C. Droz, Z. Zergoune, R. Boukadia, O. Bareille, and M. N. Ichchou, "Vibro-acoustic optimisation of sandwich panels using the wave/finite element method," *Compos. Struct.*, vol. 156, pp. 108–114, 2016.

[4] Q. Zhang *et al.*, "Bioinspired engineering of honeycomb structure - Using nature to inspire human innovation," *Prog. Mater. Sci.*, vol. 74, pp. 332–400, 2015.

[5] T. Bitzer, *Honeycomb Technology*. Dordrecht: Springer Netherlands, 1997.

[6] K. L. Alderson and K. E. Evans, "Auxetic materials: the positive side of being negative," *Eng. Sci. Educ. J.*, vol. 9, no. 4, pp. 148–154, Aug. 2000.

[7] A. Alderson *et al.*, "Elastic constants of 3-, 4- and 6-connected chiral and anti-chiral honeycombs subject to uniaxial in-plane loading," *Compos. Sci. Technol.*, vol. 70, no. 7, pp. 1042–1048, 2010.

[8] K. E. Evans and A. Alderson, “Auxetic Materials: Functional Materials and Structures from Lateral Thinking!,” *Adv. Mater.*, vol. 12, no. 9, pp. 617–628, May 2000.

[9] L. J. Gibson and M. F. Ashby, *Cellular solids. Structure and properties.* 1997.

[10] D. Zenkert, *The handbook of sandwich construction*. London: EMAS publishing, 1997.

[11] R. G. Dabbs, “Advanced Materials in Future Aircraft Design,” *Aircr. Eng. Aerosp. Technol.*, vol. 47, no. 1, pp. 21–24, Jan. 1975.

[12] J. Huang, X. Gong, Q. Zhang, F. Scarpa, Y. Liu, and J. Leng, “In-plane mechanics of a novel zero Poisson’s ratio honeycomb core,” *Compos. Part B Eng.*, vol. 89, pp. 67–76, 2016.

[13] T.-C. Lim, *Auxetic Materials and Structures*. Singapore: Springer Singapore, 2015.

[14] T. A. M. Hewage, K. L. Alderson, A. Alderson, and F. Scarpa, “Double-Negative Mechanical Metamaterials Displaying Simultaneous Negative Stiffness and Negative Poisson’s Ratio Properties,” *Adv. Mater.*, no. September, pp. 1–10, Oct. 2016.

[15] X. Hou and V. V. Silberschmidt, “Metamaterials with Negative Poisson’s Ratio: A Review of Mechanical Properties and Deformation Mechanisms,” 2015, pp. 155–179.

[16] R. Lakes, “Advances in negative Poisson’s ratio materials,” *Adv. Mater.*, vol. 5, no. 4, pp. 293–296, Apr. 1993.

[17] A. Bezazi, F. Scarpa, and C. Remillat, “A novel centresymmetric honeycomb composite structure,” *Compos. Struct.*, vol. 71, no. 3–4, pp. 356–364, 2005.

[18] K. E. EVANS, M. A. NKANSAH, I. J. HUTCHINSON, and S. C. ROGERS, “Molecular network design,” *Nature*, vol. 353, no. 6340, pp. 124–124, Sep. 1991.

[19] J. N. Grima, “New auxetic materials, Ph.D. thesis,” University of Exeter, 2000.

[20] A. Spadoni and M. Ruzzene, “Elasto-static micropolar behavior of a chiral auxetic lattice,” *J. Mech. Phys. Solids*, vol. 60, no. 1, pp. 156–171, 2012.

[21] J. N. Grima, R. Caruana-Gauci, D. Attard, and R. Gatt, “Three-dimensional cellular structures with negative Poisson’s ratio and negative compressibility properties,” *Proc. R. Soc. A Math. Phys. Eng. Sci.*, vol. 468, no. 2146, pp. 3121–3138, Oct. 2012.

[22] Y. J. Chen, F. Scarpa, Y. J. Liu, and J. S. Leng, “Elasticity of anti-tetrachiral anisotropic lattices,” *Int. J. Solids Struct.*, vol. 50, no. 6, pp. 996–1004, 2013.

[23] D. Prall and R. S. Lakes, “Properties of chiral honeycombe with Poisson’s ratio of -1,” *Int. J. Mech. Sci*, vol. 39, no. 3, 1997.

[24] C. Lira, P. Innocenti, and F. Scarpa, “Transverse elastic shear of auxetic multi re-entrant honeycombs,” *Compos. Struct.*, vol. 90, no. 3, pp. 314–322, 2009.

[25] F. Scarpa and P. J. Tomlin, “On the transverse shear modulus of negative Poisson’s ratio honeycomb structures,” *Fatigue Fract. Eng. Mater. Struct.*, vol. 23, no. 8, pp. 717–720, 2000.

[26] F. SCARPA and G. TOMLINSON, “Theoretical Characteristics of the Vibration of Sandwich Plates With in-Plane Negative Poisson’S Ratio Values,” *J. Sound Vib.*, vol. 230, no. 1, pp. 45–67, 2000.

[27] W. Miller, C. W. Smith, and K. E. Evans, “Honeycomb cores with enhanced buckling strength,” *Compos. Struct.*, vol. 93, no. 3, pp. 1072–1077, 2011.

[28] A. Alderson, K. L. Alderson, G. Chirima, N. Ravirala, and K. M. Zied, “The in-plane linear elastic constants and out-of-plane bending of 3-coordinated ligament and cylinder-ligament honeycombs,” *Compos. Sci. Technol.*, vol. 70, no. 7, pp. 1034–1041, 2010.

[29] K. E. Evans, “The design of doubly curved sandwich panels with honeycomb cores,” *Compos. Struct.*, vol. 17, no. 2, pp. 95–111, Jan. 1991.

[30] R. LAKES, “Foam Structures with a Negative Poisson’s Ratio,” *Science (80).*, vol. 235, no. 4792, pp. 1038–1040, Feb. 1987.

[31] I. G. Masters and K. E. Evans, “Models for the elastic deformation of honeycombs,” *Compos. Struct.*, vol. 35, no. 4, pp. 403–422, 1996.

[32] W. Miller, C. W. Smith, F. Scarpa, and K. E. Evans, “Flatwise buckling optimization of hexachiral and tetrachiral honeycombs,” *Compos. Sci. Technol.*, vol. 70, no. 7, pp. 1049–1056, 2010.

[33] A. Lorato *et al.*, “The transverse elastic properties of chiral honeycombs,” *Compos. Sci. Technol.*, vol. 70, no. 7, pp. 1057–1063, 2010.

[34] P. Bettini, A. Airoldi, G. Sala, L. Di Landro, M. Ruzzene, and A. Spadoni, “Composite chiral structures for morphing airfoils: Numerical analyses and development of a manufacturing process,” *Compos. Part B Eng.*, vol. 41, no. 2, pp. 133–147, 2010.

[35] J. Martin, J. J. Heyder-Bruckner, C. Remillat, F. Scarpa, K. Potter, and M. Ruzzene, “The hexachiral prismatic wingbox concept,” *Phys. Status Solidi Basic Res.*, vol. 245, no. 3, pp. 570–577, 2008.

[36] A. Airoldi, P. Bettini, P. Panichelli, and G. Sala, “Chiral topologies for composite morphing structures - Part II: Novel configurations and technological processes,” *Phys. status solidi*, vol. 252, no. 7, pp. 1446–1454, Jul. 2015.

[37] A. Spadoni, M. Ruzzene, and F. Scarpa, “Dynamic Response of Chiral Truss-core Assemblies,” *J. Intell. Mater. Syst. Struct.*, vol. 17, no. 11, pp. 941–952, 2006.

[38] M. Ruzzene, L. Mazzarella, P. Tsopelas, and F. Scarpa, “Wave Propagation in Sandwich Plates with Periodic Auxetic Core,” *J. Intell. Mater. Syst. Struct.*, vol. 13, no. 9, pp. 587–597, 2002.

[39] Y. Ma, F. Scarpa, D. Zhang, B. Zhu, L. Chen, and J. Hong, “A nonlinear auxetic structural vibration damper with metal rubber particles,” *Smart Mater. Struct.*, vol. 22, no. 8, p. 84012, 2013.

[40] M. M. Shokrieh and M. S. Mazloomi, “An analytical method for calculating stiffness of two-dimensional tri-axial braided composites,” *Compos. Struct.*, vol. 92, no. 12, pp. 2901–2905, 2010.

[41] S. Torquato, L. V. Gibiansky, M. J. Silva, and L. J. Gibson, “Effective mechanical and transport properties of cellular solids,” vol. 97, pp. 31–33, 1997.

[42] G. C. Saha, A. L. Kalamkarov, and A. V. Georgiades, “Asymptotic homogenization modeling and analysis of effective properties of smart composite reinforced and sandwich shells,” *Int. J. Mech. Sci.*, vol. 49, no. 2, pp. 138–150, 2007.

[43] I. Chekkal, M. Bianchi, C. Remillat, F.-X. Bécot, L. Jaouen, and F. Scarpa, "Vibro-Acoustic Properties of Auxetic Open Cell Foam: Model and Experimental Results," *Acta Acust. united with Acust.*, vol. 96, no. 2, pp. 266–274, Mar. 2010.

[44] C. Lira, F. Scarpa, and R. Rajasekaran, "A Gradient Cellular Core for Aeroengine Fan Blades Based on Auxetic Configurations," *J. Intell. Mater. Syst. Struct.*, vol. 22, no. 9, pp. 907–917, 2011.

[45] M. Ranjbar, L. Boldrin, F. Scarpa, S. Neild, and S. Patsias, "Vibroacoustic optimization of anti-tetrachiral and auxetic hexagonal sandwich panels with gradient geometry," *Smart Mater. Struct.*, vol. 25, no. 5, p. 54012, 2016.

[46] A. Ajdari, H. Nayeb-hashemi, and A. Vaziri, "Dynamic crushing and energy absorption of regular , irregular and functionally graded cellular structures," *Int. J. Solids Struct.*, vol. 48, no. 3–4, pp. 506–516, 2011.

[47] A. Alderson, K. L. Alderson, S. A. Mcdonald, B. Mottershead, S. Nazare, and P. J. Withers, "Piezomorphic Materials," *Macromol. Mater. Eng.*, pp. 318–327, 2013.

[48] T. C. Lim, "Functionally graded beam for attaining poisson-curving," *J. Mater. Sci. Lett.*, vol. 21, no. 24, pp. 1899–1901, 2002.

[49] C. Lira and F. Scarpa, "Transverse shear stiffness of thickness gradient honeycombs," *Compos. Sci. Technol.*, vol. 70, no. 6, pp. 930–936, 2010.

[50] Y. Hou, Y. H. Tai, C. Lira, F. Scarpa, J. R. Yates, and B. Gu, “The bending and failure of sandwich structures with auxetic gradient cellular cores,” *Compos. Part A Appl. Sci. Manuf.*, vol. 49, pp. 119–131, 2013.

[51] T.-C. Lim, “Buckling and vibration of circular auxetic plates,” *J. Eng. Mater. Technol.*, vol. 136, no. 6, p. 21007, 2014.

[52] B. T. Maruszewski, A. Drzewiecki, R. Starosta, and L. Restuccia, “Thermoelastic damping in an auxetic rectangular plate with thermal relaxation: Forced vibrations,” *J. Mech. Mater. Struct.*, vol. 8, no. 10, pp. 403–413, 2013.

[53] X. Shiyin, H. Xiuchang, and H. Hongxing, “A study on the isolation performance of trichiral lattices with gradient geometry,” *J. Vib. Control*, vol. 21, no. 16, pp. 3465–3475, 2015.

[54] S. Marburg, “Developments in structural acoustic optimization for passive noise control,” pp. 291–370, 2002.

[55] B. Howell, P. Prendergast, and L. Hansen, “Examination of acoustic behavior of negative poisson’s ratio materials,” *Appl. Acoust.*, vol. 43, no. 2, pp. 141–148, Jan. 1994.

[56] M. Ruzzene, “Vibration and sound radiation of sandwich beams with honeycomb truss core,” *J. Sound Vib.*, vol. 277, no. 4–5, pp. 741–763, 2004.

[57] S. Marburg, H. J. Beer, J. Gier, H. J. Hardtke, R. Rennert, and F. Perret, “Experimental verification of structural-acoustics modeling and design optimization,” *J. Sound Vib.*, vol. 252, no. 4, pp. 591–615, 2002.

[58] M. Tinnsten, “Optimization of acoustic response — a numerical and experimental comparison,” pp. 122–129, 2000.

[59] K. Svanberg, “The method of moving asymptotes-a new method for structural optimization,” *International Journal for Numerical Methods in Engineering*, vol. 24, no. 2. pp. 359–373, 1987.

[60] M. Ranjbar, S. Marburg, and H. J. Hardtke, “Structural-acoustic optimization of a rectangular plate: A tabu search approach,” *Finite Elem. Anal. Des.*, vol. 50, pp. 142–146, 2012.

[61] M. Ranjbar, “Fast Vibroacoustic Optimization of Mechanical Structures Using Artificial Neural Networks,” *Int. J. Mech. Eng. Appl.*, vol. 1, no. 3, p. 64, 2013.

[62] S. M. M. Ranjbar, “Vibroacoustical Optimization of Mechanical Structures Using Geometry Modification Concept and Genetic Algorithm Method,” *J. Mech. Eng. Tarbiat Modares Univ.*, vol. 12, no. 2, pp. 134–143, 2012.

[63] M. Ranjbar and S. Marburg, “Vibroacoustic Optimization of Mechanical Structures: A Controlled Random Search Approach,” *Adv. Mater. Res.*, vol. 622–623, pp. 158–161, Dec. 2012.

[64] M. Ranjbar, S. Marburg, and H. J. Hardtke, “A New Hybrid Design of Experiments Approach for Optimization in Structural Acoustics,” *Appl. Mech. Mater.*, vol. 110–116, pp. 5015–5020, Oct. 2011.

[65] M. Ranjbar, H.-J. Hardtke, D. Fritze, and S. Marburg, “Finding The Best Design Within Limited Time: A Comparative Case Study On Methods For Optimization In Structural Acoustics,” *J. Comput. Acoust.*, vol. 18, no. 2, pp. 149–164, Jun. 2010.

[66] K. Svanberg, “A class of globally convergent optimization methods based on conservative convex separable approximations,” *SIAM J. Optim.*, vol. 12, no. 2, pp. 555–573, 2002.

[67] Swanson Analysis System Inc, “ANSYS.” Academia Research, Release 14.

[68] M. Grediac, “A finite element study of the transverse shear in honeycomb cores,” *Int. J. Solids Struct.*, vol. 30, no. 13, pp. 1777–1788, 1993.

[69] F. G. Kollmann, *Maschinenakustik-grundlagen, meßtechnik, berechnung, beeinflussung*, 2nd revise. Berlin: Springer-Verlag, 2000.

[70] D. Fritze, S. Marburg, and H. J. Hardtke, “Estimation of radiated sound power: A case study on common approximation methods,” *Acta Acust. united with Acust.*, vol. 95, no. 5, pp. 833–842, 2009.

[71] J. H. Holland, *Adaptation in Natural and Artificial Systems.* Ann Arbor, MI: University of Michigan Press, 1975.

[72] K. F. Man, K. S. Tang, and S. Kwong, "Genetic algorithms: Concepts and applications," *IEEE Trans. Ind. Electron.*, vol. 43, no. 5, pp. 519–534, 1996.

[73] C. R. Houck and M. G. Kay, "A Genetic Algorithm for Function Optimization : A Matlab Implementation," *Ncsuie Tr*, vol. 95, no. 919, pp. 1–14, 2008.

[74] M. S. Mazloomi, M. Ranjbar, L. Boldrin, F. Scarpa, S. Patsias, and N. Ozada, "Vibroacoustics of 2D Gradient Auxetic Hexagonal Honeycomb Sandwich Panels," *Compos. Struct.*, 2017.

APPENDICES

Appendix A: Element Properties

SHELL 63 Elements

SHELL63 is an elastic shell elements which has both bending and membrane capabilities. Both in-plane and normal loads are permitted. The element has six degrees of freedom at each node: translations in the nodal x, y, and z directions and rotations about the nodal x, y, and z axes. Stress stiffening and large deflection capabilities are included. A consistent tangent stiffness matrix option is available for use in large deflection (finite rotation) analyses. See Section 14.63 of the ANSYS Theory Reference for more details about this element. Similar elements are SHELL43 and SHELL181 (plastic capability), and SHELL93 (mid-side node capability). The ETCHG command converts SHELL57 and SHELL157 elements to SHELL63 [67].

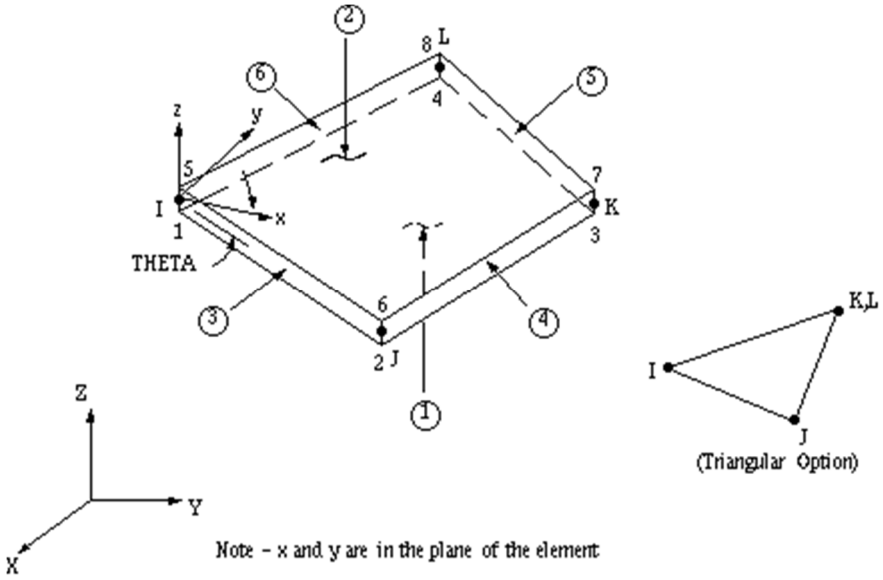

Figure 52: SHELL63 geometry and node locations [67]

The geometry, node locations, and the coordinate system for this element are shown in Figure 52. The element is defined by four nodes, four thicknesses, an elastic foundation stiffness, and the orthotropic material properties. Orthotropic material directions correspond to the element coordinate directions. The element coordinate

system orientation is as described in Section 2.3. Properties not input default as described in Section 2.4. The element x-axis may be rotated by an angle THETA (in degrees).

The thickness is assumed to vary smoothly over the area of the element, with the thickness input at the four nodes. If the element has a constant thickness, only TK(I) need be input. If the thickness is not constant, all four thicknesses must be input.

SOLID45 Elements

SOLID45 is a 3D structural solid elements which is used for the three-dimensional modeling of solid structures. The element is defined by eight nodes having three degrees of freedom at each node: translations in the nodal x, y, and z directions.

The element has plasticity, creep, swelling, stress stiffening, large deflection, and large strain capabilities. A reduced integration option with hourglass control is available. See Section 14.45 of the ANSYS Theory Reference for more details about this element. A similar element with anisotropic properties (SOLID64) is described in Section 4.64. A higher-order version of the SOLID45 element (SOLID95) is described in Section 4.95.

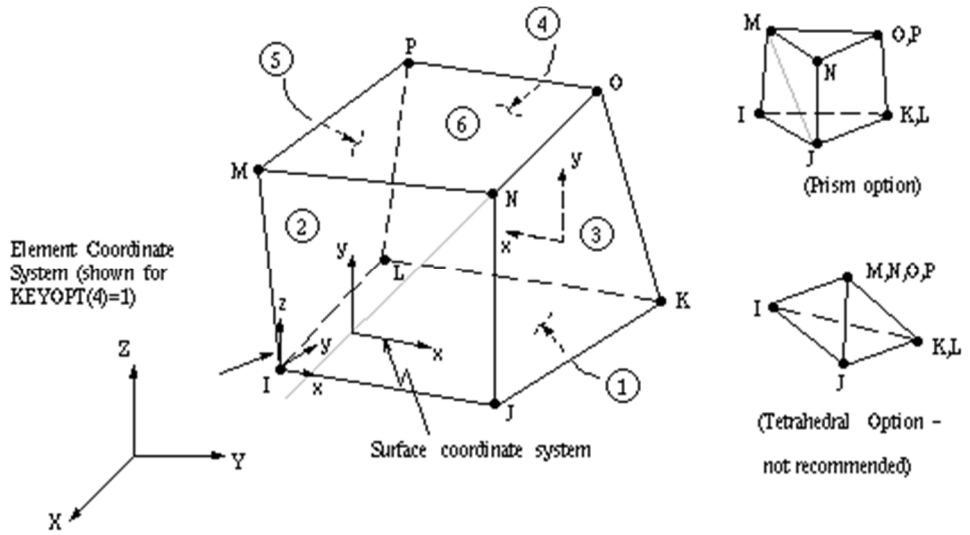

Figure 53: SOLID45 geometry and node locations [67]

The geometry, node locations, and the coordinate system for this element are shown in Figure 53The element is defined by eight nodes and the orthotropic material properties. Orthotropic material directions correspond to the element coordinate directions. The element coordinate system orientation is as described in Section 2.3. Properties not input default as described in Section 2.4.

Element loads are described in Section 2.7. Pressures may be input as surface loads on the element faces as shown by the circled numbers on Figure 4.45-1. Positive pressures act into the element. Temperatures may be input as element body loads at the nodes [67].

Appendix B: MATLAB Codes

In this appendix the MATLAB codes for genetic algorithm are shown. The first part is the code for calculating the objective function which includes integrating MATLAB and ANSYS software. The second part is GA optimization code.

Objective Function Calculation Code

```
function sam=fitnessfunction3(teta)
teta1=100*teta(1)-50;
teta2=100*teta(2)-50;
teta3=100*teta(3)-50;
teta4=100*teta(4)-50;
teta5=100*teta(5)-50;
teta6=100*teta(6)-50;
teta7=100*teta(7)-50;
teta8=100*teta(8)-50;
teta9=100*teta(9)-50;
fid= fopen('parameters.inp','w+'); %4.2f !a \n
fprintf(fid,'teta1=%f\n',teta1);
fprintf(fid,'teta2=%f\n',teta2);
fprintf(fid,'teta3=%f\n',teta3);
fprintf(fid,'teta4=%f\n',teta4);
fprintf(fid,'teta5=%f\n',teta5);
fprintf(fid,'teta6=%f\n',teta6);
fprintf(fid,'teta7=%f\n',teta7);
fprintf(fid,'teta8=%f\n',teta8);
fprintf(fid,'teta9=%f\n',teta9);
```

```
fclose(fid);
!"C:\Program Files\ANSYS Inc\v150\ansys\bin\winx64\Ansys150.exe" -b -i
FEAinnR.txt -o FEAoutR.txt
fid=fopen('objfun.txt','r');
FR=fscanf(fid,'%f',[1,1]);
fclose(fid);

sam=FR;
end
```

GA Optimization Code:

```
clc;clear all;close all;
%   DESIGN VARIABLES
%    x1   x2 x3  x4  x5  x6  x7 x8  x9
ub=[50 50 50 50 50 50 50 50 50];
lb=[-50 -50 -50 -50 -50 -50 -50 -50 -50];
xmin=lb;
xmax=ub;
nsample=50;
p=9;
eeen=ones(nsample,p);
eeen1=50*eeen;
x = lhsdesign(nsample,p)

s = (x * 100)-eeen1;
```

```
plotmatrix (s);
objfun = @fitnessfunction
%options = gaoptimset('PopInitRange',[-10,-10,-10,-10;-50,-50,-50,-50],
'Generations';10;'PopulationSize';10;)
nvars=9;
options = gaoptimset;
%% Modify options setting
options = gaoptimset(options,'PopulationSize', nsample);
options = gaoptimset(options,'InitialPopulation', s)
% options = gaoptimset(options,'PopInitRange' ,[lb;ub]);
% % options = gaoptimset('InitialPop', InitPop);
% options = gaoptimset(options,'InitialPopulation' ,[InitPop]);
% % options = gaoptimset(options,'PopInitRange' ,[InitPop]);
% % options = gaoptimset(options,'PopulationSize' ,100);
options = gaoptimset(options,'Generations' ,100);
options = gaoptimset(options,'StallGenLimit' ,100);
% options = gaoptimset(options,'TolFun' ,1e-9);
% options = gaoptimset(options,'TolCon' ,1e-9);
% options = gaoptimset(options,'StallTimeLimit' ,200000000);
options = gaoptimset(options,'CrossoverFcn' ,@crossovertwopoint);
options = gaoptimset(options,'CrossoverFraction' ,0.8);
options = gaoptimset(options,'SelectionFcn' ,{ @selectiontournament 4  });
% options = gaoptimset(options,'CrossoverFcn' ,@crossovertwopoint);
options = gaoptimset(options,'MutationFcn' ,{ @mutationuniform 0.254 });
options = gaoptimset(options,'Display' ,'iter');
```

```
% options = gaoptimset(options,'Display', 'off')
options = gaoptimset(options,'PlotFcns', { @gaplotbestf })

% LB=[-50 -50 -50 -50 -50 -50 -50 -50 -50];
% HB=[-10 -10 -10 -10 -10 -10 -10 -10 -10];
[x,fval]=ga(objfun,nvars,[],[],[],[],lb,ub,[],options);
```